

1-1-2016

Acrylonitrile Butadiene Styrene Hybrid Fuel with Radially Azimuthally Partitioned Paraffin Cells

Joseph F. St Columbia

Follow this and additional works at: <https://scholarsjunction.msstate.edu/td>

Recommended Citation

St Columbia, Joseph F., "Acrylonitrile Butadiene Styrene Hybrid Fuel with Radially Azimuthally Partitioned Paraffin Cells" (2016). *Theses and Dissertations*. 367.
<https://scholarsjunction.msstate.edu/td/367>

This Graduate Thesis - Open Access is brought to you for free and open access by the Theses and Dissertations at Scholars Junction. It has been accepted for inclusion in Theses and Dissertations by an authorized administrator of Scholars Junction. For more information, please contact scholcomm@msstate.libanswers.com.

Acrylonitrile butadiene styrene hybrid fuel with radially
azimuthally partitioned paraffin cells

By

Joseph F. St. Columbia III

A Thesis
Submitted to the Faculty of
Mississippi State University
in Partial Fulfillment of the Requirements
for the Degree of Master of Science
in Aerospace Engineering
in the Department of Aerospace Engineering

Mississippi State, Mississippi

December 2016

Copyright by
Joseph F. St. Columbia III
2016

Acrylonitrile butadiene styrene hybrid fuel with radially
azimuthally partitioned paraffin cells

By

Joseph F. St. Columbia III

Approved:

Keith Koenig
(Major Professor)

Keith Hodge
(Committee Member)

Thomas E. Lacy
(Committee Member)

J. Mark Janus
(Graduate Coordinator)

Jason Keith
Dean
Bagley College of Engineering

Name: Joseph F. St. Columbia III

Date of Degree: December 9, 2016

Institution: Mississippi State University

Major Field: Aerospace Engineering

Major Professor: Keith Koenig

Title of Study: Acrylonitrile butadiene styrene hybrid fuel with radially azimuthally partitioned paraffin cells

Pages in Study: 108

Candidate for Degree of Master of Science

Additively manufactured fuels are becoming more common in the area of hybrid rockets due to the enhanced possibilities provided by computer aided design and improved additive material technology. When integrated with a highly compliant yet energetic paraffin wax, the additive manufactured material can help support the paraffin wax during the burn, and improve overall performance. This study investigates thin-walled acrylonitrile butadiene styrene structures that separate paraffin wax into azimuthally partitioned cells. The fuel grains are tested using a vertical test stand, custom nitrous system, and data acquisition system. The computer program Chemical Equilibrium with Applications is used to compare common hybrid fuels such as sorbitol, polybutadiene acrylic acid acrylonitrile, and poly(methyl methacrylate) along with the manufactured fuel. The experimental results indicate the promise of higher performance using paraffin. The analyses, however, show that refinements in grain design are necessary to fully realize the advantages of paraffin.

DEDICATION

This thesis is dedicated to my family, friends, colleagues, the Council, and Mary Clay Bailey who supported me throughout my undergraduate and graduate studies, especially my grandmother, Joyce St. Columbia. She always told me to pursue my dreams, and to believe that anything is possible.

ACKNOWLEDGEMENTS

I would first like to thank Dr. Keith Koenig for serving as my academic advisor during my undergraduate and graduate studies at Mississippi State University (MSU). Without Dr. Koenig providing his guidance, support, and mentorship, I wouldn't be the man or the engineer I am today. I would also like to thank Dr. Thomas E. Lacy and Dr. B. K. Hodge for their advice, reviews, and evaluation on my masters' thesis.

Thank you to the MSU Aerospace Department for providing a family-like environment and atmosphere for the past six years. My time and experiences at Mississippi State University wouldn't have been the same without the caring faculty and staff in the ASE department. Thank you providing me support to help me reach my goals and ambitions.

Lastly, I would like to thank the MSU hybrid propulsion team for enduring all of the labor and hard work required for the solid and hybrid test fires. Honoring the attitude of "failure is not an option", these gentleman kept the program on track for my research and are committed to future hybrid testing at MSU.

TABLE OF CONTENTS

DEDICATION	ii
ACKNOWLEDGEMENTS	iii
LIST OF TABLES	vii
LIST OF FIGURES	ix
NOMENCLATURE	xii
CHAPTER	
I. INTRODUCTION	1
II. FUEL MANUFACTURING	3
2.1 Fuel Selection	3
2.2 Additive Material Selection	3
2.2.1 3D Printer	4
2.2.2 3D Printer File Settings	6
2.3 Fuel Geometry	7
2.3.1 Rectilinear (Printer Defined) Geometry	7
2.3.2 Radial Azimuthally Geometry	12
2.4 Paraffin Wax Selection and Processing	15
2.5 ABS/Paraffin Fuel Integration	16
2.5.1 First Generation Paraffin Casting Assembly	16
2.5.2 Second Generation Paraffin Casting Assembly	20
III. TEST HARDWARE	28
3.1 Propellant Integration	28
3.2 Multipurpose Solid/Hybrid Vertically Integrated Test Stand	30
3.2.1 Test Stand Hardware	31
3.2.2 Oxidizer Flow Control System	33
3.3 Thrust Data Acquisition System	34
3.3.1 Hardware/Sensor Package	35
3.3.2 DAQ Software	37
3.4 Solid and Hybrid Test Procedures	38

IV.	CHEMICAL EQUILIBRIUM WITH APPLICATOIN ANALYSIS	40
4.1	Introduction to CEA	40
4.1.1	Program Input	40
4.1.1.1	Problem Section.....	41
4.1.1.2	Reactant Section	44
4.1.1.3	Output	46
4.2	Heat of Formation.....	47
4.2.1	Group Addition Method	47
4.3	Propellant Types	49
4.3.1	Nitrous Oxide	50
4.3.2	Sorbitol	50
4.3.3	Poly(methyl methacrylate) (PMMA)	51
4.3.4	Polybutadiene Acrylic Acid Acrylonitrile (PBAN)	52
4.3.5	Paraffin Wax.....	54
4.3.6	Acrylonitrile Butadiene Styrene (ABS).....	56
4.4	Similar Hybrid Studies Using CEA.....	59
4.4.1	CEA Enthalpy and Pressure Simulations	60
4.4.2	CEA Rocket Problem Simulations	63
4.5	Performance Predications	64
V.	TEST RESULTS	68
5.1	Data Extraction Software	68
5.2	Results	68
5.2.1	Preliminary Test Fire Results	70
5.2.2	ABS/Paraffin Test Fire Results	72
5.2.3	Specific Impulse Estimation.....	77
VI.	LESSONS LEARNED	81
6.1	Hardware Modifications.....	81
6.1.1	Hybrid Motor Casing.....	81
6.1.2	Nitrogen Oxide Feed System.....	83
6.1.3	Horizontal Test Stand.....	83
6.2	Fuel Modifications.....	84
6.2.1	Azimuthally and Axially Partitioned Cells.....	85
6.2.2	Helical Design	86
6.3	Conclusion.....	87
	REFERENCES	88
	APPENDIX	
A.	RADIAL FUEL GRAIN CALCULATIONS.....	93
B.	SOILD/HYBRID TEST PROCEDURES	95

C.	VAN KREVLAN GROUP CONTRIBUTIONS.....	99
D.	PARAFFIN HEAT OF FORMATION CALCULATIONS.....	101
E.	CHIMEI CORPORATION PA-747 GENERAL ABS.....	103
F.	THRUST EXTRACTION MATHCAD PROGRAM.....	105
G.	EIGHT AND SIXTEEN CELL TEST FIRE.....	107

LIST OF TABLES

2.1	PLA, ABS, and HIPS Thermal Properties and Cost	4
2.2	TAZ 5/6 Specifications.....	6
2.3	Printer Estimated and Actual Mass Comparison.....	9
2.4	ABS Volume Displacement Study for Rectilinear Pattern.....	10
2.5	ABS Volume Displacement Study for Cell Pattern	13
2.6	Paraffin Wax Physical Characteristics	16
2.7	Filled Grain Masses.....	27
3.1	Nozzle, Injector, Relief Bulkhead, and Casing Selection	29
4.1	Enthalpy and Entropy Coefficients	48
4.2	PMMA Heat of Formation Calculations	52
4.3	Heat of Formation of Paraffin Wax C_nH_{2n+2}	56
4.4	Heat of Formation of ABS Calculation.....	58
4.5	MSU and USU ABS Heat of Formation Calculations Comparison.....	59
4.6	User Selected CEA Fuel Characteristic.....	59
4.7	Enthalpy and Pressure CEA Input.....	61
4.8	NASA Ames Rocket Problem Conditions	63
4.9	MSU Rocket Problem.....	65
5.1	Solid/Hybrid Test Fire Log	69
5.2	Hybrid Test Results	76
5.3	Burn Time and Post Burn Nitrous Flow Time Comparison.....	78

5.4	Performance Calculations.....	79
-----	-------------------------------	----

LIST OF FIGURES

2.1	TAZ 6 by LULZBOT	5
2.2	Rectilinear Fuel Modeled in CURA at 20% ABS Fill	8
2.3	Printed Rectilinear Fuel at Different ABS Percent Fills	9
2.4	Sample Rectilinear Fuel at 10% ABS after Test Fire.....	11
2.5	2D Models of the Four, Eight, Sixteen, and Thirty-Two Cell Design	12
2.6	4 Cell CURA Model.....	13
2.7	Sample 8 Cell Pattern after Test Fire	14
2.8	A) Paraffin Wax and B) Carbon Black.....	16
2.9	First Generation Paraffin/ABS Integration System 2D Schematic	17
2.10	First Generation Casting System Before, During, and After Fill	19
2.11	2 nd Generation ABS/Paraffin Integration System 2D Schematic	21
2.12	3D CAD Drawing of the Second Generation Fuel ABS/Paraffin Casting System	22
2.13	Second Generation Casting System Overview	24
2.14	2 nd Generation Casting System Time-lapse.....	25
2.15	Unprocessed ABS/Paraffin Fuel Grain Extraction.....	26
2.16	Processed Fuel Grains	27
3.1	Exploded and Assembly CAD Drawing.....	28
3.2	MSHVITS Top Plate CAD Assembly.....	32
3.3	MSHVITS Assembly Before Testing.....	33
3.4	Oxidizer Control Flow System 2D Diagram	34

3.5	DAQ Hardware and Sensor Package.....	36
3.6	Functional Block Diagram	36
3.7	Block Diagram of Thrust Acquisition Program	38
3.8	Front Panel of the Thrust Acquisition Program	38
4.1	CEA Problem Selection Screen With Oxidizer Dataset.....	41
4.2	CEA Hp Case	42
4.3	CEA Rocket Problem Window	44
4.4	CEA Reactant Window	45
4.5	CEA Reactant Selector Window	45
4.6	Output Window	47
4.7	Sorbitol’s Chemical Structure $C_6H_{14}O_6$	50
4.8	PMMA’s Chemical Structure. $(C_5O_2H_8)_n$	51
4.9	PBAN Chemical Structure, $C_{10}H_{13}NO_2$	53
4.10	Paraffin Wax Chemical Structure $C_{25}H_{52}$	54
4.11	Paraffin’s Generic Chemical Structure, C_nH_{2n+2}	55
4.12	ABS Chemical Structure, $(C_3H_3N C_4H_6 C_8H_8)_n$	57
4.13	CEA Hp: Adiabatic Flame Temperature for Paraffin and ABS	61
4.14	CEA Hp: Molecular Weight for Paraffin and ABS.....	62
4.15	CEA Hp: Specific Heat Ratio for Paraffin and ABS.....	62
4.16	[44] Specific Impulse with Selected Fuels	64
4.17	Exit Performance Conditions at 4000 kPa.....	66
5.1	J760 Thrust Curve Comparison.....	70
5.2	K321 Thrust Curve Comparison [46].....	71
5.3	“K321 Short” Thrust Curves	72
5.4	Unfiltered Four Cell Fuel Thrust Curves.....	73

5.5	Filtered Four Cell Fuel Thrust Curves.....	73
5.6	Eight Cell Filtered Thrust Curve.....	74
5.7	Sixteen Cell Filtered Thrust Curve.....	75
5.8	Four, Eight, Sixteen Cell Thrust Comparison.....	76
5.9	Images from Video Footage of the Four Cell Test Fire.....	77
5.10	CEA Impulse and Tested Impulse Comparison.....	80
6.1	New Hybrid Casing Concept.....	82
6.2	Igniter System.....	83
6.3	Aerocon Systems' Horizontal/Vertical Test Stand.....	84
6.4	Isometric and Cross-sectional View of the Azimuthally and Axially Four Cell Partitioned Design.....	85
6.5	Four Cell Helical Design.....	86
A.1	Radial Fuel Grain Calculations.....	94
G.1	Eight Cell Test Fire.....	108
G.2	Sixteen Cell Test Fire.....	108

NOMENCLATURE

ABS	Acrylonitrile Butadiene Styrene
A_c	Combustion Chamber Area
A_e	Exit Area
A_t	Nozzle Throat Area
ARPAL	Aerospace Rapid Prototyping Advance Lab
CAD	Computer-Aided Design
CEA	Chemical Equilibrium with Applications
CSV	Comma Separated Value
F	Thrust, lbf
GUI	Graphical User Interface
HIPS	High Impact Polystyrene
hp	Combustion (Enthalpy and Pressure)
HTPB	Hydroxyl-Terminated Polybutadiene
I	Total Impulse, lbf·s
I_{sp}	Specific Impulse, s
MSHVITS	Multipurpose Solid Hybrid Vertically Integrated Test Stand
N_2O	Nitrous Oxide
NASA	National Aeronautical Space Administration
NIST	National Institute of Standards and Technology

O/F	Oxidizer to Fuel Mass Flow Ratio
PBAN	Polybutadiene Acrylic Acid Acrylonitrile
PMMA	Poly(methyl methacrylate)
PLA	Poly(lactic acid)
R	Gas Constant, J/kg-K
rkt	Rocket Problem
SPG	Space Propulsion Group
TAP	Thrust Acquisition Program
ΔG	Gibb's Free Energy, kJ/mol
ΔG_f	Free Enthalpy of Formation, kJ/mol
$\Delta G_{f,corrections}$	Free Enthalpy of Formation Corrections, kJ/mol
$\Delta G_{f,group}$	Free Enthalpy of Formation Group Contributions, kJ/mol
ΔG_{poly}	Free Enthalpy for Polymer, kJ/mol
ΔH	Mole Specific Enthalpy, kJ/mol
ΔS	Mole Specific Entropy, kJ/mol-K

CHAPTER I

INTRODUCTION

Since the early 1930s, hybrid rocket motors combined the advantages and disadvantages of the growing market of solid and liquid propellants. The first hybrid recorded work was made by Sergie Korolev and Mikhail Tikhonravov in 1933 using gelled gasoline and liquid oxygen [1]. From this early work hybrid motors have progressed slowly when compared to their solid and liquid counterparts due to the research required and the disadvantage of low-burn, or regression rates. Increase in hybrid development of the motor occurred in the 1960s, but the regression rate problem was still a concern until the late 1980s. When the challenger disaster occurred, NASA supported research to replace the solid rocket boosters with hybrid boosters. This renewed interest in hybrid motors led to several advancements of fuels including: hydroxyl-terminated polybutadiene (HTPB), polybutadiene acrylic acid acrylonitrile (PBAN), poly(methyl methacrylate) (PMMA), and paraffin wax. Of these fuels paraffin wax appears to be the most energetic, but loses its performance due to its physical characteristics when burned. These advancements ultimately lead to the commercialization of hybrid rocket motors. Scaled Composites' SpaceShipOne, which won the Ansari X Prize, was the first successful manned rocket using hybrid propulsion. SpaceShipOne and Virgin Galactic's SpaceShipTwo use a form of HTPB as the fuel with nitrous oxide as the oxidizer. Virgin Galactic considered using an

improved nylon fuel to replace HTPB in 2014, but later claimed the original HTPB fuel to be more efficient than the nylon fuel [2].

Virgin Galactic's switch to the plastic fuel nylon was not unprecedented. During the past 20 years, universities and research groups have experimented with nylon, PMMA, and 3D-printed materials such as Acrylonitrile Butadiene Styrene (ABS). ABS shows regression rates similar to HTPB, but with slightly reduced overall performance [3]. In contrast, early research with paraffin wax as a hybrid fuel showed to be highly energetic when compared to the rubber and plastic analogs. Space Propulsion Group (SPG) is currently experimenting with a paraffin-based fuel for which the regression rate is 3-5 times higher than HTPB [4]. However, paraffin loses its structural integrity when burned which ultimately leads to a loss of performance of the fuel.

The proposed research will try to enhance the paraffin fuel by adding a plastic structure to increase the structural integrity of the fuel. The plastic structure would first be 3D printed, and the paraffin would later be cast inside the structure using a custom vacuum chamber. Chemical Equilibrium Analysis (CEA) will be used to predict the performance of ABS and paraffin, and then compare them to other hybrid fuels. The ABS and paraffin dual fuel would then be test fired. A data acquisition system will gather thrust values and these values would then be compared to the theoretical calculations.

CHAPTER II

FUEL MANUFACTURING

2.1 Fuel Selection

The hybrid fuels chosen for this study was selected for the following reasons: affordability, readily available, historically used as fuel for hybrids, and easily maintained. These desired characteristics led to the selection of using two hybrid fuels: additive manufacturing material and paraffin wax. Additive manufacturing is the process of creating an object from a 3D model usually using a layer by layer process; it allows one to create almost any geometry for the fuel with some slight limitations in regard to the equipment capabilities [5]. While additive manufactured materials such as metals or plastics would allow one to create any geometry for fuel, the material itself is not that energetic when compared to other hybrid fuels. In contrast, paraffin wax has been regarded as one of the most energetic hybrid fuels, but is hard to form as a fuel and maintained. If combined together, an additive manufactured material and paraffin wax would make an ideal fuel combination for a hybrid motor.

2.2 Additive Material Selection

Since affordability and practicality were main characteristic for fuel selection, metals, thermosetting resins, and glass additive materials were excluded in the fuel selection. This exclusion left the following thermoplastics as the frontrunners: polyactic acid (PLA), acrylonitrile butadiene styrene (ABS), polyvinyl alcohol (PVA), and high

impact polystyrene (HIPS). Table 2.1 shows the thermal properties and costs of these three plastics.

Table 2.1 PLA, ABS, and HIPS Thermal Properties and Cost

Characteristic	PLA	ABS	HIPS
Extrusion Temperature (°C)	175 -200	230 - 240	230 - 250
Bed Temperature (°C)	45 - 70	225	50 - 60
Price* (USD/kg)	\$43	\$43	\$25

Note: * values from Village Plastics [6].

PLA is made from either sugar cane or a starch which allows it to be an environmentally favorable biodegradable print, but it is known to be very brittle when impacted. In contrast, HIPS is derived from polystyrene and typically used for prototyping parts due to its low cost, structural characterizes, and aesthetic properties. Of the three plastics, ABS was chosen due to its overall structural advantages and thermal properties than the other two plastics; however, ABS does contain acrylonitrile and butadiene which are anticipated or known to be carcinogenic to humans. [7] [8] The possible carcinogens would be a threat during fuel combustion only, and not while printing/manufacturing the fuel; ABS's extrusion temperature is lower than the temperature at which ABS fully decomposes into acrylonitrile and butadiene above 400°C. [9]

2.2.1 3D Printer

The ABS structure of the fuel was formed in the Mississippi State University (MSU) Aerospace Rapid Prototyping Advance Lab (ARPAL). ARPAL was outfitted with

two new three-dimensional (3D) printers purchased specifically to manufacture fuel grains that could be 11 in (279 mm) in height and 3.85 in (98 mm) in diameter. The printers chosen were LULZBOT's TAZ 5 and TAZ 6 3D printers. The TAZ printers have the capability to print in many plastic materials with options of water soluble material and dual extrusion capabilities [10]. Figure 2.1 shows a TAZ 6 after finishing a test print. Table 2.2 lists the specifications for both TAZ printers.



Figure 2.1 TAZ 6 by LULZBOT

Note: Image from reference [10].

Table 2.2 TAZ 5/6 Specifications

Physical Dimensions (in)	Print Bed Dimensions (in)	Weight (lbf)	Average Print Speed (in/s)	Materials Used
26 x 20.47 x 20.47	11 x 11 x 9.8	43	1.18 – 1.97	ABS, HIPS, PLA, NGEN

Note: Specifications from reference [10].

The two printers are virtually identical, although with a few operational differences. The newer model, TAZ 6, automatically cleans the extruder, levels the bed, and informs the operator when the print is ready for bed removal. The TAZ 5 does not perform any of these automatic features, but still maintains ease of operation.

2.2.2 3D Printer File Settings

Once the plastic material is selected, and the printer’s extruder and bed plate are preheated to the proper temperature for a specific material, a G-code file must be uploaded to the TAZ printer to initiate the print. In order to create a G-code file, computer aided drawing (CAD) software can be used to create a model, but the stereolithography (STL) file from the CAD program must then be sent to a slicing software program. The slicing program used by the TAZ printers, CURA, allows the printer settings to be applied to the model which in turn creates the G-code file.

CURA allows the user to select the following parameters: shell thickness, fill type, support type, removal of top and bottom layers, and print speed. Some parameters such as print speed can directly affect the quality of the part (i.e., the higher the speed the lower the quality of the part, and vice versa). The constant factory recommended speed of 25

mm/s was used for all fuel prints to ensure the highest quality part. Once the final part configuration was defined, the cura model file is then saved and uploaded to the printer for manufacturing.

2.3 Fuel Geometry

The ABS fuel geometry considered in this study primarily focused on a center bore geometry with ABS partitions which were thereafter filled with paraffin wax. The fuel geometry was selected to be 9 in (228.6 mm) in height and 1.91 inches (48.5 mm) in diameter so that it could be enclosed in a standardized 54mm hybrid casing. Even though the height of the fuel could have been increased to 10 or 11 inches, the printer's quality for these part dimensions degraded and therefore a 9 in tall fuel was chosen.

2.3.1 Rectilinear (Printer Defined) Geometry

A rectilinear pattern was derived using CURA's built in percentage fill patterns to automatically create ABS partitions for the paraffin. These patterns were initially designed to reduce the amount of material required to create the part, while keeping the structural integrity. Many 3D printer hobbyists use this tool to lower both the cost to print each part and the time required to print each part [11]. Figure 2.2 shows an example of the fuel modeled at 20% fill. The yellow squares represent the toolpath of the print extruder that define the ABS partitions. The volume between partitions will be filled with paraffin.

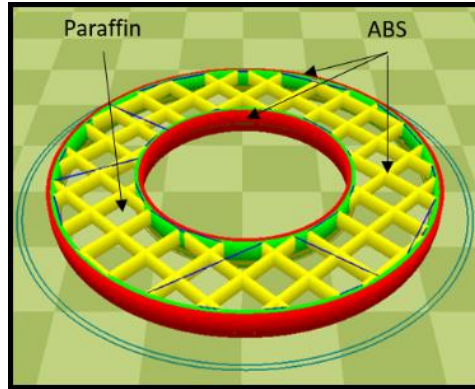


Figure 2.2 Rectilinear Fuel Modeled in CURA at 20% ABS Fill

The rectilinear ABS cell wall geometry allowed an automated grid system that would change with the varying fill in density of ABS. Initially the concept was to print 90%, 50%, 25%, and 10% ABS fuel with 10%, 50%, 75%, and 90% paraffin, respectively. 100% ABS fuel were excluded due to its excessive print time (i.e. over 24 hours) as opposed to the 18 hours of a 90% ABS fuel. However, the ABS fuel's 90% rectilinear grid was filled solid due to the small tolerance of the printer extruder and very small partitions. Therefore, a 75% grain replaced the 90% grain in the sample selection. 5.5 in (139.7 mm) fuel samples were printed and then weighed to verify the 3D printer's weight calculation was accurate. Unfortunately, the actual mass of each fuel sample was not equal to the estimated mass, raising the question of whether the printer's percent fill calculations were accurate. Figure 2.3 shows each type of grain not filled with paraffin while Table 2.3 shows the weight comparison of the estimated prints and the actual weight.

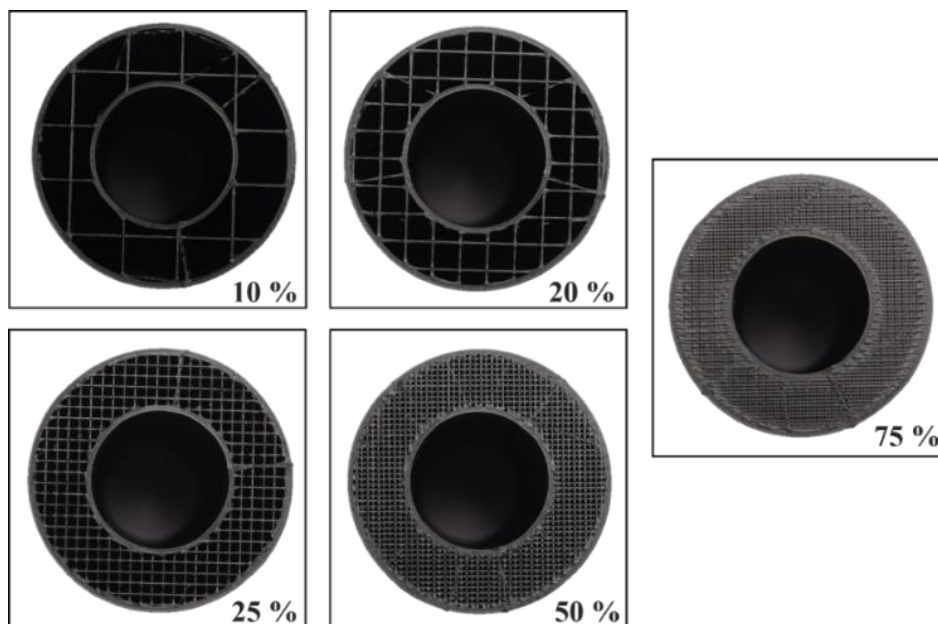


Figure 2.3 Printed Rectilinear Fuel at Different ABS Percent Fills

Table 2.3 Printer Estimated and Actual Mass Comparison

ABS Percent Fill (%)	Printer Mass (g)	Actual Mass (g)	Error (%)
10	54	51	5.6
20	72	68	5.6
25	81	76	6.2
50	125	117	6.4
75	170	158	7.1

Due to the inaccuracy of CURA’s calculation of the ABS’s mass, a volume displacement study was performed to ensure the ABS percent fill calculated by CURA was accurate. A 2.2 inch (55.88 mm) diameter graduated cylinder was used to verify the percentage fill. The cylinder was first filled with 500 mL of room temperature water, and the solid fuel was submerged into the cylinder and agitated until air bubbles were not present. The change in volume was recorded which represented the actual volume of the

ABS fuel. This value was then divided by the calculated volume of a 100% ABS cylinder (187.45 mL) and multiplied by 100 to find the actual ABS percent fill. Additionally, the volume of the paraffin partitions was calculated by subtracting the actual volume of the ABS fuel from the calculated volume of a 100% fill ABS fuel. Table 2.4 shows the results of this experiment.

Table 2.4 ABS Volume Displacement Study for Rectilinear Pattern

Estimated Printer ABS Percent Fill (%)	Actual ABS Percent Fill (%)	Error of Percent Fill (%)	Actual ABS Volume (mml)	Actual Paraffin Volume (mml)
10	27	167	50	137
20	37	87	70	117
25	48	92	90	97
50	64	28	120	67
75	85	14	160	27

The study showed CURA’s method of calculating the ABS percent fill of the fuel is incorrect. Table 2.4 shown above, depicts the deviation of the estimated ABS percent fills of 75%, 50%, 25%, 20%, and 10% were off from the actual ABS percent fills by 85%, 64%, 48%, 37% and 27% respectively. Since this study required a wide range of percent fills, high ABS content/low paraffin content and low ABS content/ high paraffin content, a new practice to create fuel grains was needed to satisfy this requirement.

While this new practice was under development, preliminary tests were conducted with the rectilinear pattern fills. These tests included: verifying print qualities between parts, filling the ABS partitions with paraffin, and testing the fuel. From print to print the parts never changed mass or percent fill. Filling the partitions with paraffin proved to be a challenge at first. Directly poring the paraffin into the ABS structure allowed air pockets

to exist. A vacuum method of casting the paraffin inside the ABS structure was created to mitigate the air pockets inside the fuel. The test firing of these fuels did reveal some interesting characteristic of ABS and paraffin which can be seen in Figure 2.4.

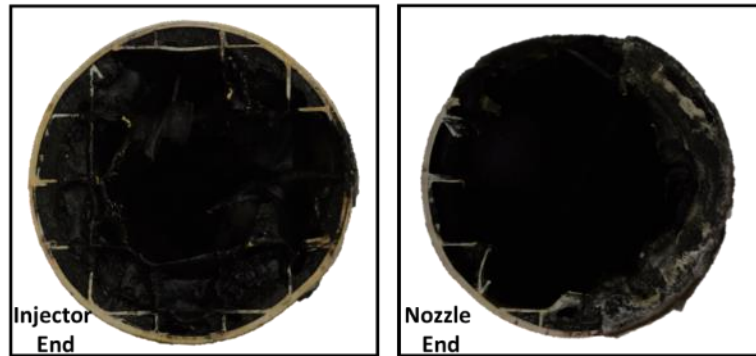


Figure 2.4 Sample Rectilinear Fuel at 10% ABS after Test Fire

The tests fires of these fuel patterns were performed using nitrous oxide, N_2O , as the oxidizer. The tests showed that the combustion of the fuel was both incomplete and asymmetric, seen in Figure 2.4. The lower ABS partitions in the images of Figure 2.4 were unburnt compared to the upper ABS partitions. The injector end of the ABS/paraffin fuel did not completely burn, which was expected, but did reveal a problem with this fuel geometry. When the fuel is burning, the rectilinear geometry forces the oxidizer to first burn the ABS circular port layer, then the first of many paraffin layers, and then the ABS partitions to the subsequent paraffin layers. This layering of different materials created an instability while burning and an inefficacy of nitrous use.

2.3.2 Radial Azimuthally Geometry

Due to the unpredictable rectilinear geometry and burning characteristics, a new geometry was developed in order to accurately measure the percent fill of ABS and ensure a complete stable burn of the fuel. This new geometry incorporated a radial cell pattern centered on the azimuthal axis of the fuel. This pattern allows one to manually integrate multiple cell geometries while at the same time incorporating lessons learned from the rectilinear pattern. Figure 2.5 shows a cross sectional view of the 3D models made in CATIA while Figure 2.6 shows a 4 cell design in CURA.

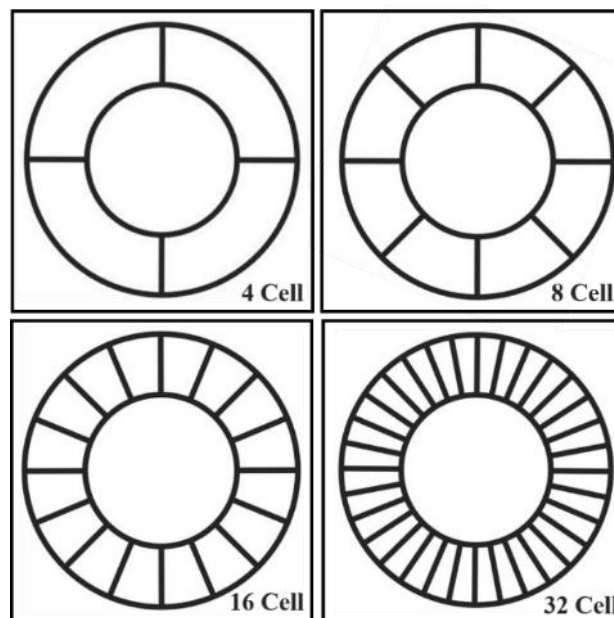


Figure 2.5 2D Models of the Four, Eight, Sixteen, and Thirty-Two Cell Design

Notes: Each fuel's CAD file was constructed by using the defined outer and inner diameter constraint of 48.514 mm (1.91 in) and 25.4 mm (1.00 in). Using these diameters, the cells were constrained by the number of partitions required and the required angular spacing. The cells depicted above have the following cell numbers and angular spacing: 4 cells at 90 degrees, 8 cells at 45 degrees, 16 cells at 22.5 degrees, and 32 cells at 11.25 degrees, respectively.

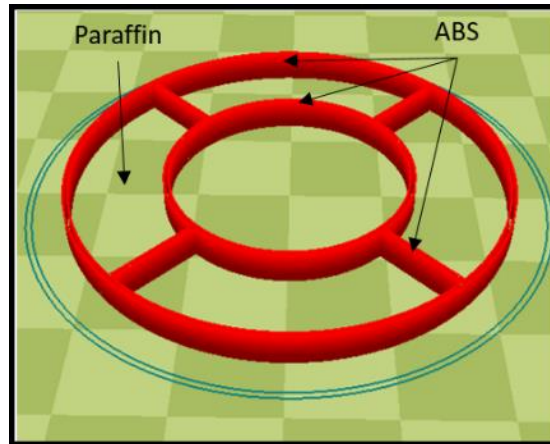


Figure 2.6 4 Cell CURA Model

The radial azimuthal geometry allowed one to completely customize the percent fill by changing the number of partitions. A sample percent fill calculations with a 1 mm wall thickness can be seen in Appendix A for a 4 cell design. Another ABS volume displacement study was performed using a 4, 8, 16, and 32 cell designs to ensure an accurate representation of percent fill and also to find the volume of the paraffin inside each cell. Table 2.5 shows the percent fill cell study.

Table 2.5 ABS Volume Displacement Study for Cell Pattern

Cell Instances	Calculated ABS Percent Fill (%)	Actual ABS Percent Fill (%)	Error (%)	Actual ABS Volume (ml)	Actual Paraffin Volume (ml)
4	20	21	6	40	147
8	23	27	16	50	137
16	28	32	11	60	127
32	40	42	6	80	107

The ABS volume displacement study shows that 4, 8, 16, and 32 cell geometries have a percent fill of 21%, 27%, 32%, and 43%. A 2 cell geometry was calculated to have a percent fill of 18.7% which is the lowest percent fill possible between these geometries. After the ABS volume displacement study was completed a similar test fire was performed to ensure a symmetric burn was achieved. An 8 cell grain was test fired with a ABS partition wall thickness to be 1 mm while the ABS shell thickness of the entire fuel grain was 1.5 mm. The shell thickness main purpose for any 3D printed part is to increase the outer surface thickness to ensure the parts durability when being handled. Figure 2.7 shows the 8 cell fuel grain after the burn.

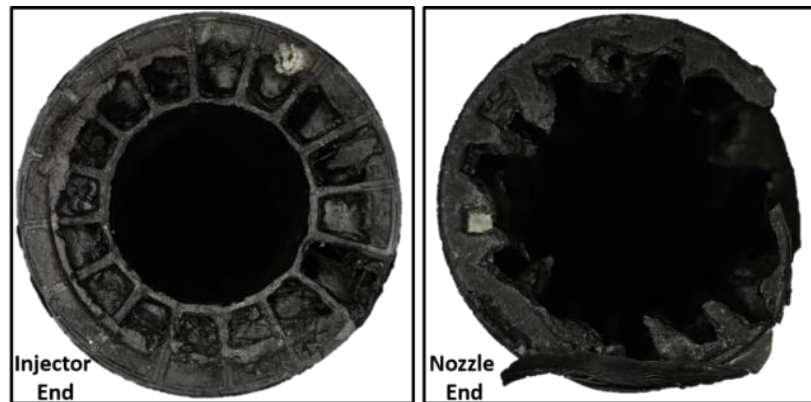


Figure 2.7 Sample 8 Cell Pattern after Test Fire

Shown in the left image of Figure 2.7, the injector end of the fuel grain shows the fuel grain's structure remained mostly unburned while continuing towards the nozzle more material was burned away. Further inspection of the grain showed several of the partitions towards the nozzle were unburned. The unburnt portions of the fuel were contributed by an irregular flow from the injector and the inner and outer shell thickness of the motor

being 1.5 mm. The injector's flow was altered due to the separation and ignition mechanism's failure to sever and ignite the N_2O supply line. This failure was later addressed to ensure separation and ignition of the oxidizer line and oxidizer, respectively. The irregular flow caused 1 in of the injector side of the fuel grain to not burn while the ABS inner shell thickness prevented paraffin burning throughout the fuel similar to the rectilinear case. The ABS inner and outer shell thickness was later reduced to 1 mm in order to ensure the inner walls of the fuel burns quickly, but also maintain structural integrity for the outer walls while burning.

2.4 Paraffin Wax Selection and Processing

The wax pertaining to this study will exclusively be petroleum based paraffin wax. This particular type of wax was chosen due to both its inherent properties as a solid at room temperature and thermodynamic properties when heated. The paraffin wax was purchased from McMaster Carr in a small pellet form and would only be melted by an indirect heat source. Since the paraffin will be injected into the ABS via a vacuum, additives could be intermixed within the paraffin prior to injection to improve performance. Carbon black to the mixture to reduce the thermal radiation through the fuel [12]. Figure 2.8 shows the pellet paraffin from McMaster Carr (A) and the carbon black (B) and Table 2.6 describes the physical properties of this paraffin wax.

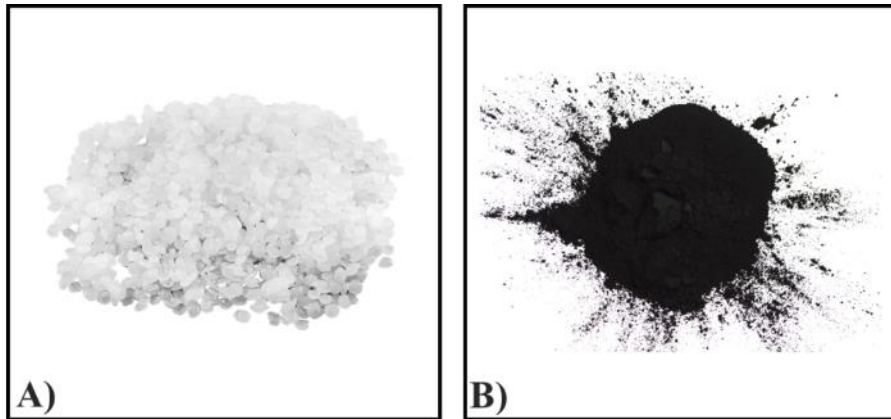


Figure 2.8 A) Paraffin Wax and B) Carbon Black

Notes: Paraffin Wax figure from reference [13]

Table 2.6 Paraffin Wax Physical Characteristics

Melting Point (°C)	Flash Point (°C)	Room Temperature Density (kg/m ³)
45 – 76 [13]	190 [13]	865– 913 [14]

2.5 ABS/Paraffin Fuel Integration

To ensure the ABS fuel grains were completely filled with paraffin with no voids, the paraffin wax was cast under a vacuum while the wax solidified. The paraffin was heated in a double boiler at a constant temperature of 60°C to ensure all contents including the additive were melted and intermixed. The carbon black was added to the mixture once the wax was fully melted, and the additive would be heavily concentrated in the solution.

2.5.1 First Generation Paraffin Casting Assembly

Since it was unknown if the ABS was porous enough for the paraffin to soak into ABS when heated, one end of the fuel would be submerged into a double boiler while the top portion of the fuel was attached to a customized vacuum chamber. The centerbore of

the fuel was not to be filled with paraffin, so a plug was created from D312 vacuum bag sealant tape sourced from Jamestown Distributors. The sealant tape was also used to seal the joint between the vacuum chamber and the fuel grain. Figure 2.9 shows a 2D schematic of this concept.

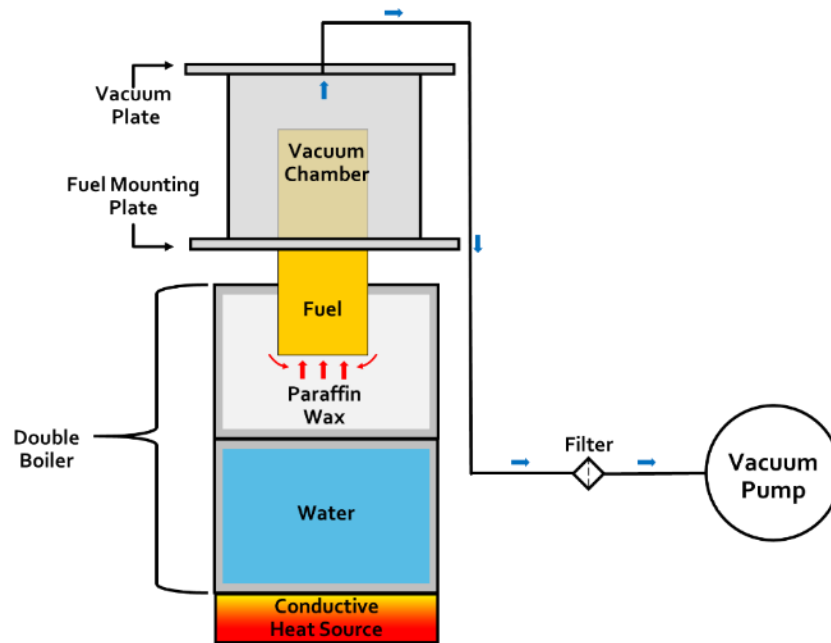


Figure 2.9 First Generation Paraffin/ABS Integration System 2D Schematic

The vacuum chamber was constructed using a repurposed 4 in inner diameter acrylic tube, a top acrylic plate fitted with a $\frac{1}{4}$ in NPTF male hose coupling, and a bottom 3D printed plate to connect the vacuum chamber and fuel grain. The vacuum chamber assembly was held together using threaded rods, wing nuts, and O-rings to ensure a tight seal. The ABS fuel was then positioned inside the vacuum chamber and then temporarily sealed using the sealant tape. The complete assembly was placed directly over the double boiler using a composite support structure, and the vacuum pump was attached using a $\frac{1}{4}$ in

female vacuum hose. Preliminary tests fills excluded carbon black for a better understanding of how paraffin behaves by itself when heated and under vacuum.

To begin fill operations, a one pound bag of paraffin was poured into the preheated double boiler and agitated to decrease the melting time. The ABS fuel mass was recorded and then the ABS fuel was inserted to the bottom vacuum plate. After attaching the ABS fuel and sealing it with sealant tape, the entire vacuum assembly with air hose and vacuum pump was integrated and checked for air escaping the system. Finally, the complete system was then placed on top of the double boiler, excluding the vacuum pump, to fill the fuel grain. All fuel grains were submerged just above the bottom of the paraffin section of the boiler so that the grain would not be drawing in air. Figure 2.10 shows the entire assembly before, during, and after the fill.

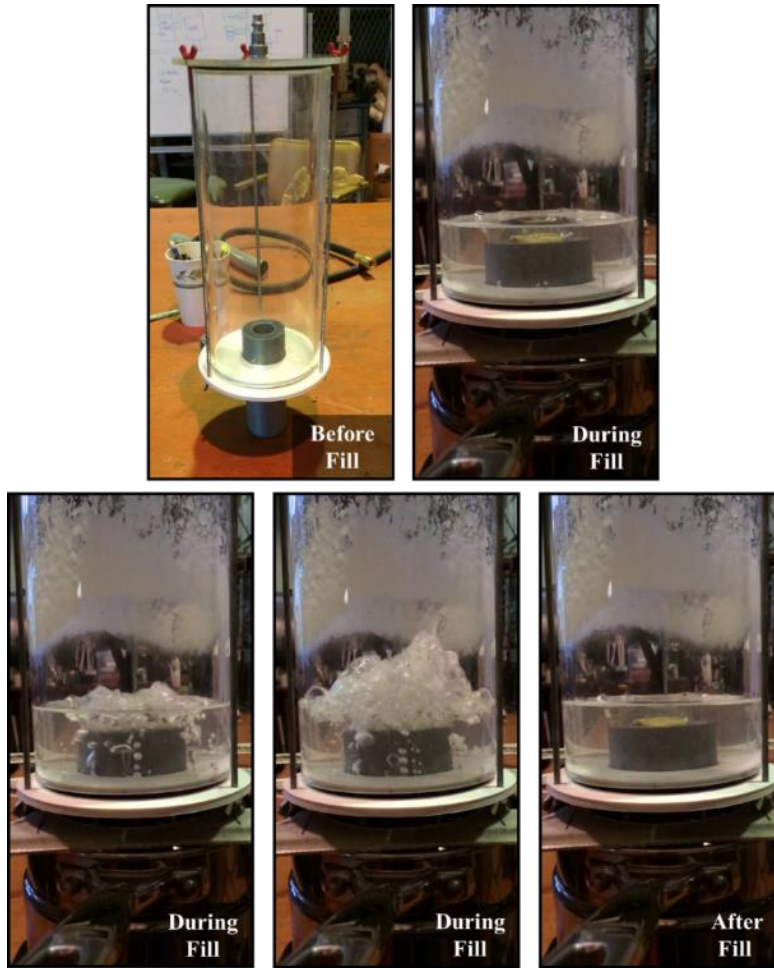


Figure 2.10 First Generation Casting System Before, During, and After Fill

Once the paraffin was melted, its viscosity was comparable to that of room temperature water. The paraffin was rapidly drawn through the ABS partitions by the vacuum pump until no paraffin remained in the double boiler. The vacuum would then only draw in air which was not desired. To fix this oversight, the vacuum pump's pressure was decreased, and a new identical ABS fuel replaced the previous ABS fuel to begin a new fill. This fill was performed with better results; however, once the pump was off the paraffin started leaking back into the double boiler. The leaking posed a major problem

because the paraffin was still hot; by the time the paraffin cooled the ABS fuel would not be filled completely with paraffin. Another major problem in this casting system was that the vacuum chamber was directly above the double boiler which by itself is not a hazard, but when not properly secured and with liquid hot paraffin inside could pose as a hazard. The last problem was that a large quantity of paraffin was used to fill a 4 in diameter vacuum chamber when only a 2 in diameter vacuum could be used to fill the ABS fuel. These three problems lead to a redesign of a new safe casting system that could fill an ABS fuel every time without voids and requires less paraffin to fill.

2.5.2 Second Generation Paraffin Casting Assembly

From the lessons learned of the first generation casting system, a similar casting system was quickly designed and fabricated to ensure safe, without voids, and economical fills every time. The new design reused similar concepts including using an acrylic tube enclosed by 3D-printed plates as a vacuum chamber, incorporating a double boiler as the reservoir to hold and heat the paraffin, and a regulating/filtered vacuum pump. However, this design included several modifications from the first casting system. The ABS fuel was still attached and sealed to the vacuum chamber via 3D-printed plates and vacuum sealant tape in between the seals of the vacuum tube and plates. The ABS fuel also incorporated a 3D-printed plug that would seal the center bore entirely instead of using the sealant tape. The 3D-printed plug was created by using two identical parts that are held together in compression by threaded rods and wing nuts. Next, a 3D-printed injector is attached to the bottom of the ABS fuel to direct the flow of the paraffin into the ABS fuel. The injector allows flow from a paraffin reservoir using a ¼ in polyurethane tubing which will be attached at the bottom portion of the injector. The addition of the injector allowed a valve

to be installed into the system. The valve was placed in between the injector and the paraffin reservoir to seal the vacuum chamber from the paraffin reservoir. Once closed, the valve restricted the paraffin from leaving the vacuum chamber, and allowing the paraffin to be cooled without creating voids in the fuel. Figure 2.11 shows a 2D drawing of the new system.

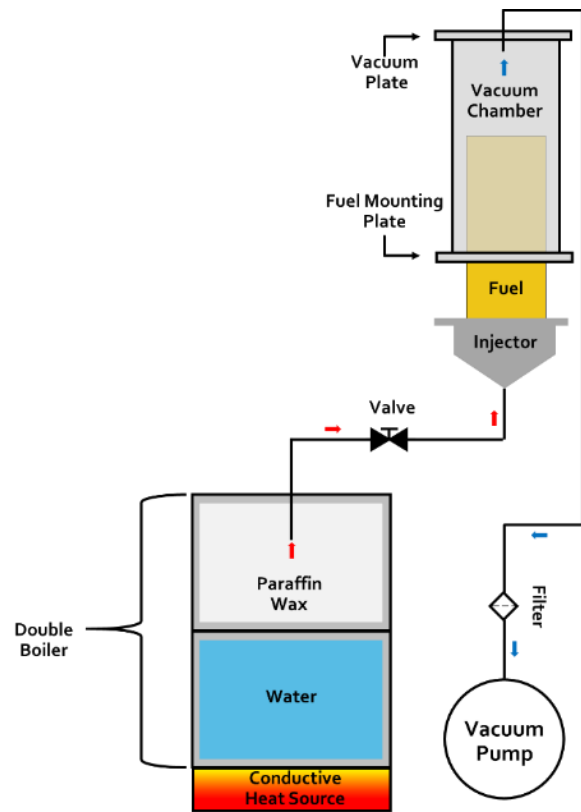


Figure 2.11 2nd Generation ABS/Paraffin Integration System 2D Schematic

The design change allowed most of the parts to be easily printed including the vacuum plate, fuel mounting plate, fuel grain plug, and paraffin injector while a new vacuum tube, polyurethane tubing, and a PVC ball valve was purchased from McMaster

Carr. The new vacuum tube was chosen to be a 2 in inner diameter by 1 ft tall acrylic tube to decrease the amount of paraffin required to fill a fuel grain by half. The polyurethane tubing and PVC ball valve were selected to use a ¼ in diameter tubing to create uniformity in tubing size throughout the casting system. In addition, if a smaller tube diameter was used the paraffin would have a higher chance of cooling before getting to the injector. Figure 2.12 shows a 3D model of the new vacuum system (left) and the cross sectional flow path of the paraffin (right).

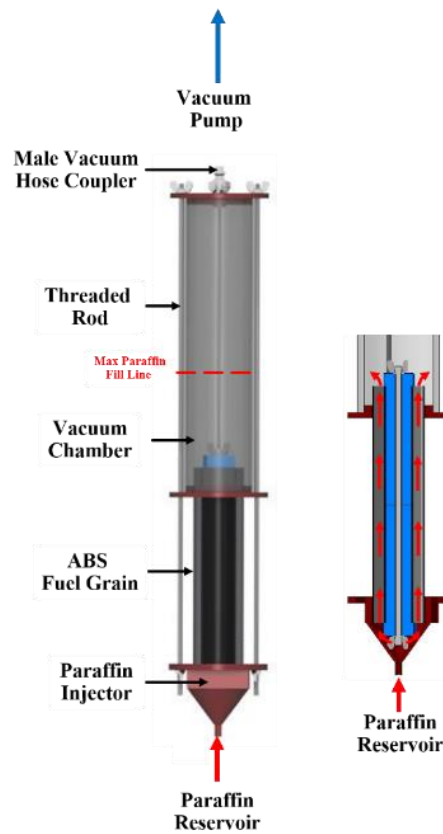


Figure 2.12 3D CAD Drawing of the Second Generation Fuel ABS/Paraffin Casting System

The casting assembly was first integrated by aligning the vacuum plate and fuel plate with the vacuum chamber with respect to the threaded rod guide holes. The ABS fuel was then inserted, with plug already installed, one in into the vacuum chamber. The paraffin injector was the attached to the bottom of the fuel grain and aligned to the other threaded rod guide holes. The sealant tape was then adhered to the fuel grain plate/fuel grain joint and the paraffin injector/fuel grain joint, and the threaded rods and wing nuts were used to compress the entire structure. Aluminum tubes were added in between the fuel grain plate and injector to help compress the entire system. After the casting assembly was integrated, the assembly was then attached to a vertical mounting bracket. Once attached to the structure, the polyurethane tubing and PVC ball valve were then connected and tested to ensure there were no leaks in the system. Finally, the tubing was placed inside the paraffin reservoir and the vacuum hose was attached to the vacuum hose coupler.

The fill process for the new system was kept similar to the previous system with minor changes. The system was first checked with no leaks and the fuel grain was inspected beforehand. The paraffin wax was melted at 60°C and mixed with the carbon black. The polyurethane tubing was then placed inside the paraffin/carbon black solution, and the solution was agitated to ensure all contents going into the fill are completely mixed. The vacuum pump was then turned on and the paraffin/carbon black filled the polyurethane tubing and enter the vacuum chamber. Once enough paraffin/carbon black has been filled into the chamber, the PVC valve was then closed and the vacuum chamber was then turned off. The joints of chamber and fuel grain were then inspected for any leaks of paraffin/carbon black and the assembly was set to cool at room temperature. Figure 2.13 shows the entire system while Figure 2.14 shows a time lapse of the fill.

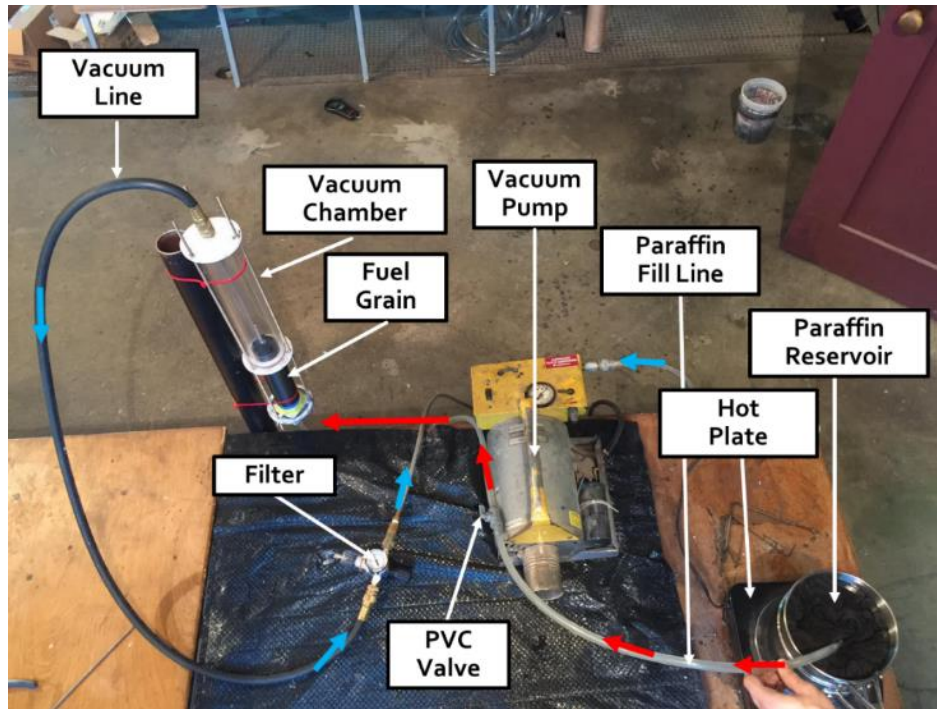


Figure 2.13 Second Generation Casting System Overview

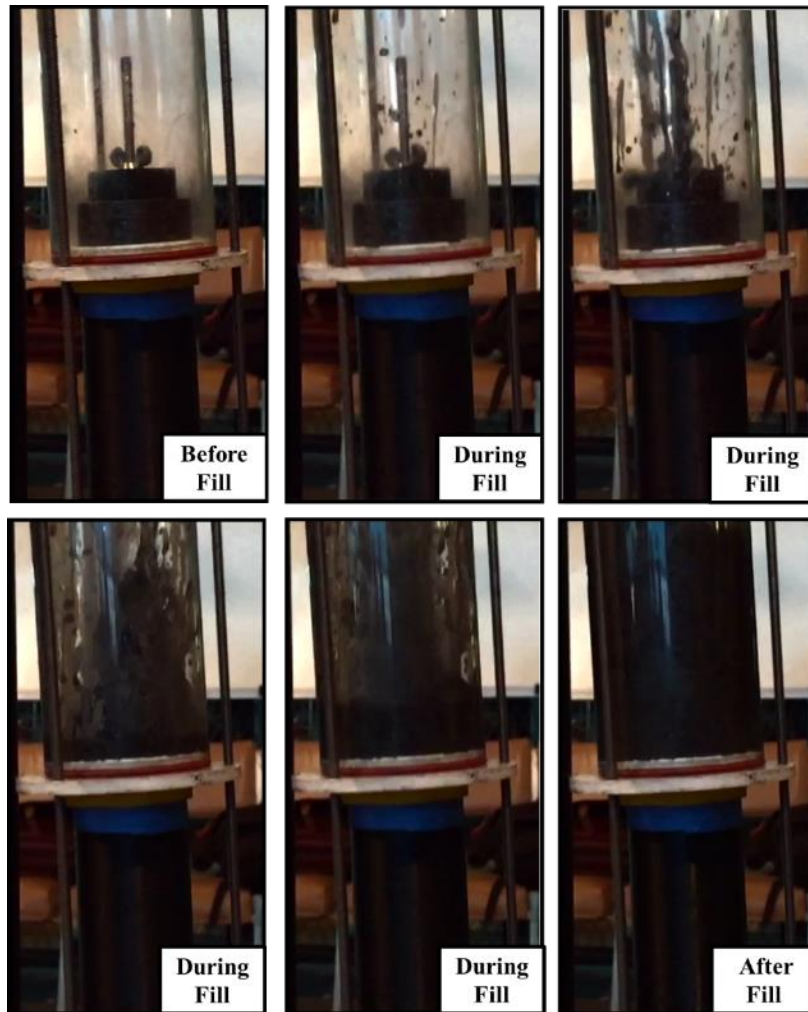


Figure 2.14 2nd Generation Casting System Time-lapse

Once cooled the grain was then extracted from the vacuum chamber by hand. First the threaded rods and sealant tape were removed which allowed the vacuum plate and injector to be removed. Next, the vacuum chamber was easily removed by torqueing it azimuthally. The vacuum chamber removal was surprisingly easy since paraffin's physical characteristics allow it to be removed when adhered to the inner glossy finished surface of the vacuum chamber. The paraffin injector was removed a similar fashion. Figure 2.15

shows the removal of all the vacuum assembly and the paraffin filled ABS fuel waiting to be processed.

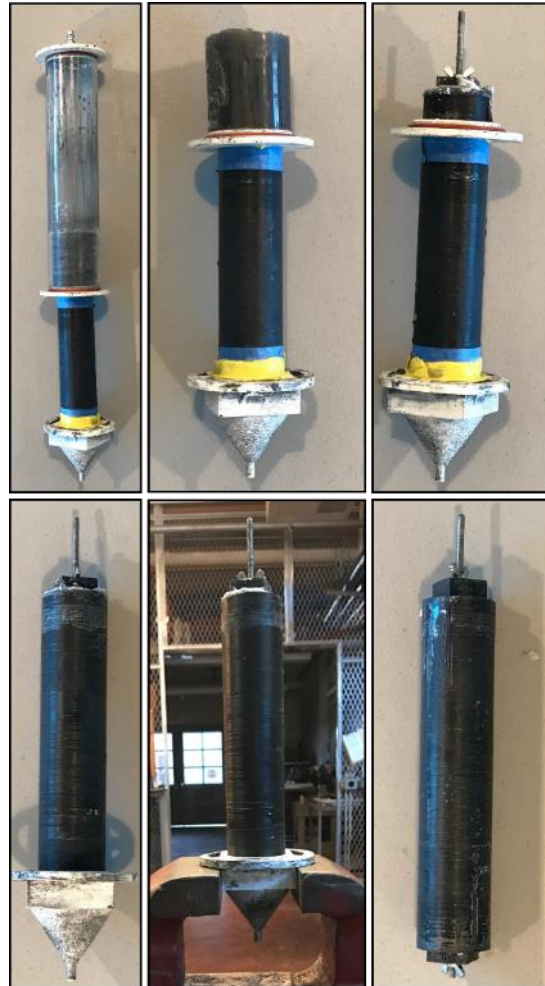


Figure 2.15 Unprocessed ABS/Paraffin Fuel Grain Extraction

After the paraffin/ABS fuel was removed from the vacuum assembly, the fuel was processed manually to meet testing standards. These standards were defined as follows: the grain must have a clean center bore, with no voids in the fuel grain, and not show physical damage. At the ends of each fuel, excess paraffin was removed using a sharp blade to the

ABS mold and then the fuel was inspected for voids. Next the centerbore was inspected and trimmed by using a 3D printed plunger. Finally, the fuels were weighed and cataloged in Table 2.7. Figure 2.16 shows the 4, 8, and 16 cell fuels after processing.

Table 2.7 Filled Grain Masses

Fuel Geometry	ABS Printed Mass (grams)	ABS/ Paraffin Average Filled Mass (grams)
4 Cell	67	290
8 Cell	77	285
16 Cell	96	285



Figure 2.16 Processed Fuel Grains

Though each fuel has a different printed mass shown in Table 2.7, when injected with paraffin and carbon black the average mass of each type of grain was very similar. This similarity in mass was due to paraffin's ability to bleed into any cracks of the printed ABS structure. The bleeding of the paraffin occurred inside the partitions as well as the outside of the fuel grain. Fortunately when the outside bleeding occurred, the paraffin would quickly cool and seal when in contact of ambient room temperature.

CHAPTER III
TEST HARDWARE

3.1 Propellant Integration

A commercially available hybrid casing was used to integrate the ABS/paraffin fuel with a predefined nozzle, injector, and oxidizer tank. The hybrid casing chosen was Contrail Rocket's 54mm diameter and 48 in length hybrid motor casing; it was chosen for its simplicity and ease of use. The 48 in casing uses an interchangeable design containing a nozzle, fuel, injector, and vent bulkhead which are held inside using snap rings. The casing also uses a built in oxidizer reservoir where the oxidizer can be fed through the injector. The casing's original purpose was to house a 12 in tall fuel; however, since the 3D printers limited the fuel's height to 9 in, the oxidizer reservoir of the casing increased in volume. An exploded CAD drawing of the system can be seen in Figure 3.1 and the nozzle, injector size, vent bulkhead, and casing specifications used can be seen in Table 3.1.

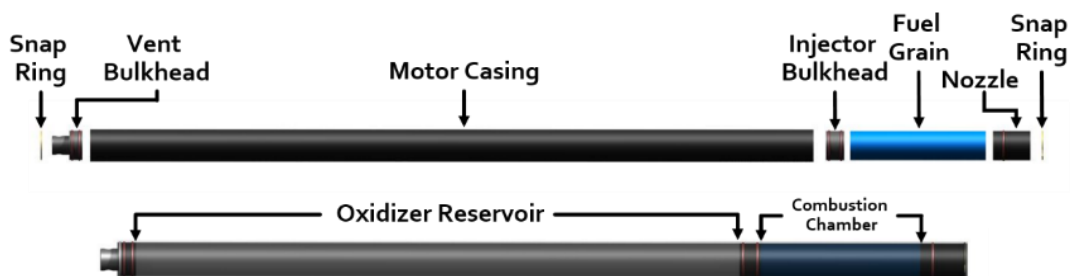


Figure 3.1 Exploded and Assembly CAD Drawing

Table 3.1 Nozzle, Injector, Relief Bulkhead, and Casing Selection

Nozzle	
Outer Diameter (mm)	48.9
Combustion Diameter (mm)	34.1
Exit Diameter (mm)	36.3
Length (mm)	64.4
Number of O-Rings	1
Injector Bulkhead	
Outer Diameter (mm)	48.9
Length (mm)	38.1
Number of O-Rings	2
Parker Valve and Tubing	
Valve Threading	1/8 NPT
Tube OD (in)	1/4
Tubing Size (in)	0.17
Tubing Burst Pressure (psi)	1000
Relief Bulkhead	
Outer Diameter (mm)	48.9
Total Length (mm)	50.8
Inside Length (mm)	22.0
Number of O-Rings	2
Parker Valve and Tubing	
Valve Threading	1/8 NPT
Tube OD (in)	1/4
Tubing Size (in)	0.17
Tubing Burst Pressure (psi)	1000
Casing	
Length (m)	1.219
Outer Diameter (mm)	54.585
Inner Diameter (mm)	48.9
With 12 inch Fuel Grain	
Oxidizer Volume (mL)	324.4
With 9 inch Fuel Grain	
Oxidizer Volume (mL)	356.0

The integration of the fuel grain and motor assembly followed Conrail Rocket's hybrid motor reload assembly manual [15]. Before integrating the motor assembly, all parts (including the fuel) were inspected and cleaned to eliminate unwanted debris inside the combustion chamber. O-rings were first installed onto the nozzle, injector, and vent

bulkhead, and then coated with Krytox™ to ensure each part would give a proper seal to the system. Next the feed/ignition system was to be constructed by using the injector bulkhead, a ¼ in to ⅛ in NPT Parker press lock valve, and a ¼ inch tubing. The press lock valve was threaded into the ⅛ in NPT injector bulkhead, and the ¼ inch nylon tubing was pushed into to the Parker valve. Each fitting was checked to ensure a tight fit otherwise a misfire would occur. Next using electrical tape, two Pyrodex pellet charge assemblies were attached to the nylon tubing as close as possible to the valve/hose joint and perpendicularly from the feed tubing. A Pyrodex pellet charge assembly contained two 50/50 caliber Pyrodex pellets and an electrical match. The manual [15] advises one Pyrodex pellet charge assembly per firing, but early testing showed that misfires or improper oxidizer flow would occur when only one charge assembly was used. After the feed/ignition system was created a small coat of white lithium synthetic grease was applied to the injector bulkhead and was inserted at one end of the motor casing. The fuel and nozzle were then coated with Mobil 1 synthetic grease and inserted after the feed/ignition bulkhead. The feed/ignition bulkhead, fuel, and nozzle were then sealed in place with the snap ring. Finally, the vent bulkhead was attached to a ⅛ in to ⅛ in NPT Parker press lock valve which will later be attached to a ⅛ in nylon tubing to release the oxidizer to atmosphere. The vent bulkhead was then coated with white lithium grease, inserted into the opposing end of the nozzle section of the casing, and sealed using a snap ring.

3.2 Multipurpose Solid/Hybrid Vertically Integrated Test Stand

To test the manufactured fuel grains, Mississippi State University's Multipurpose Solid/Hybrid Vertically Integrated Test Stand (MSHVITS) and commercial 54mm hybrid casings were used to facilitate all hybrid testing. The test stand has the capability of firing

38 - 98 mm diameter hybrid or solid propellant motors, and was outfitted with a new data acquisition system to measure the thrust of the hybrid fuel and an oxidizer flow control system.

3.2.1 Test Stand Hardware

MSHVITS was designed in 2009 with the purpose of vertically testing solid and hybrid motors of various sizes [16]. MSHVITS contains an all steel vertical frame that can be constrained to a concrete platform using ratchet straps. A frictionless motor mounting system was attached on the outer steel frame to allow a solid/hybrid motor to be integrated to MSHVITS, but also to allow the motor vertical translation. The motor mounting system uses two steel ball bearing rails mounted to the vertical outer-facing surfaces of the main support structure, and four linear ball bearings attached to a rocket motor mounting plate to ensure a frictionless vertical translation. Stops were also added as a safety and convenience to the top and bottom of both rails to prevent undesired motion of the rocket motor mounting plate. A worm gear winch pulley system was chosen to move the rocket motor mounting plate due to the winches high gear ratio and self-locking ability [16] . The high gear ratio allows the mounting plate to be adjusted with high precision so a force sensor can be loaded with just a few pounds of force. On top of the steel frame and on the same side as the ball bearing system, an aluminum top plate was mounted and outfitted with a force sensor mounting system that allows various motor sizes to be fired. The aluminum top plate was slotted down the center to allow the sensor to be positioned for a particular motor size. This sensor mounting assembly and top mounting was updated during testing to a more practical and stronger all carbon steel design due to an unexpected malfunction of one the experimental fuel grains. The new sensor mounting assembly used

three plates placed held in compression by hexagonal screws (set A shown in Figure 3.2) while a second set of hexagonal screws (set B also shown in Figure 3.2) would be adjusted to translate the sensor mounting assembly along the top mounting plate. Once set to the desired position the second set of hexagonal screws were then compressed into the top mounting plate. Figure 3.2 shows 3D-CAD drawings of the MSHVITS system and Figure 3.3 shows test stand front (left) and side (right) view after the hybrid motor is integrated.

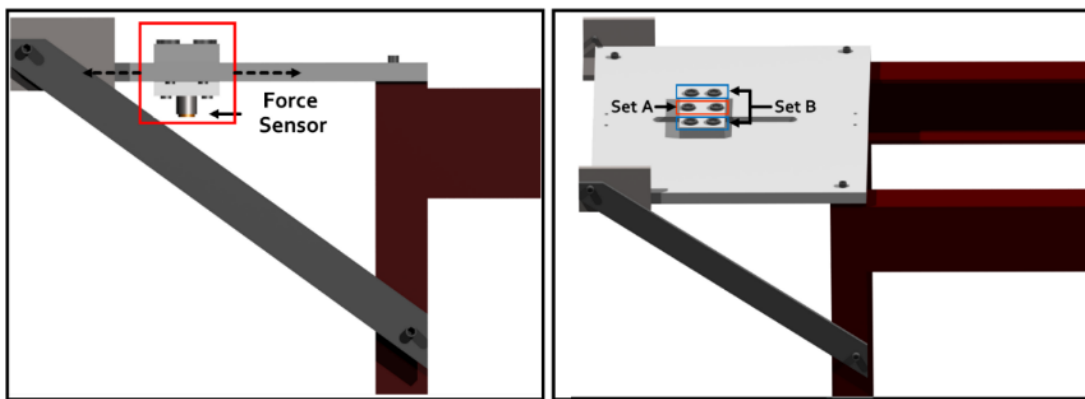


Figure 3.2 MSHVITS Top Plate CAD Assembly

Notes: The left image depicts the force sensor assembly and the force sensor being able to translate along the center of the top plate while the right image shows the two different sets of hexagonal screw to compress the sensor platform together and to set the platform in a fixed position.



Figure 3.3 MSHVITS Assembly Before Testing

3.2.2 Oxidizer Flow Control System

To convert the solid vertical test stand to a hybrid vertical test stand, a new ground support system and an oxidizer flow control system was developed to manually feed and purge the hybrid motor of nitrous oxide, N_2O . The feed/purge system allowed ground personal to manually fill the on board N_2O tank reservoir and purge the entire system in case of any potential hazards to the test stand or surrounding facilities. The oxidizer flow control system's components were designed with liquid and gaseous N_2O , and used automotive racing solenoids, high-pressure hoses, and appropriately rated plumbing fittings. Inside the flow control system were two high-pressure solenoids that could independently be actuated via the ground support control system. The solenoid configuration was chosen from the automotive racing field where a high-flow purge and standard-flow fill solenoid are placed in parallel. Before the fill solenoid was opened to

allow motor oxidizer filling, the purge solenoid was first used to purge any air or moisture from the lines. After the purge, the fill valve was open to fill in the motor casing's on-board N_2O reservoir. The addition of a purge solenoid gave the oxidizer control flow system the ability to quickly release and depressurize oxidizer lines in the case of a motor burn anomaly, with complete supply tank discharge if needed. Any purged oxidizer was bled off through low-pressure lines away from both the vertical test stand and ground control personnel. Figure 3.4 shows a 2D schematic of the oxidizer flow system.

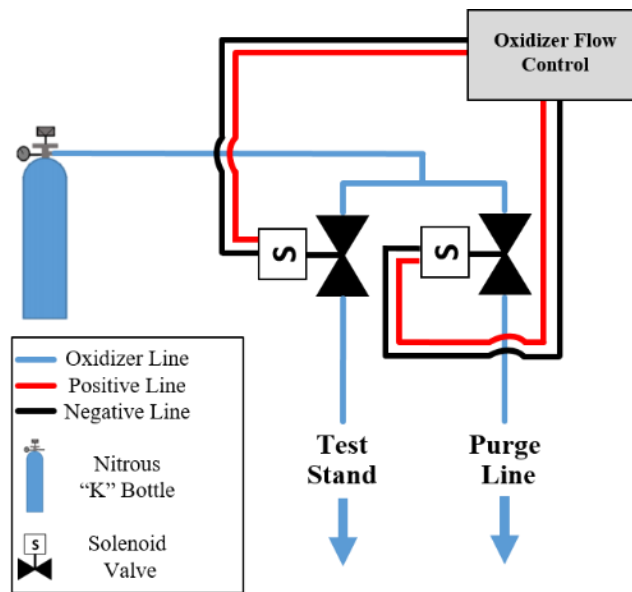


Figure 3.4 Oxidizer Control Flow System 2D Diagram

3.3 Thrust Data Acquisition System

The data acquisition (DAQ) system used in all testing was an improved version of the system used in previous hybrid testing [16]. The data acquisition system uses a custom LABVIEW program and user interface that records the thrust data from a PCB Piezotronics

force sensor. The DAQ system, oxidizer flow control system, and vertical test stand was then tested to verify the MSHVITS's safety. The validity of the test stand and motor was then compared to commercially available solid and hybrid data.

3.3.1 Hardware/Sensor Package

The previous DAQ system and components used in the 2009 hybrid tests [16] was either repurposed or found to be nonfunctional; it was decided a new DAQ system was needed. Similar to the 2009 setup, a PCB Piezotronics' 208C04 ICP force sensor was chosen to measure the thrust profile of the motors due to its compression range and high frequency range of 1000 lbf (4.448 kN) and 36 kHz, respectively. Since PCB Piezoelectric force sensors operate on a standard bias voltage, a DC-coupled signal conditioner was required to operate the force sensor. When a force is applied to the force sensor, the piezoelectric crystal inside the sensor produces a small voltage and when added to the bias voltage yields the signal voltage. This signal voltage, q , decays as a function of time which can be seen in equation 3.1. [17]

$$q = Q \cdot e^{\left(\frac{-t}{DTC}\right)} \quad (3.1)$$

Equation 3.1 shows the signal voltage is equal to the initial signal voltage, Q , multiplied by an exponential time, t , divided by the discharge time constant, DTC term. The DTC , measured in seconds, represents the time required for the sensor to discharge to 37% of the initial voltage [17]. To account for the DTC , a PCB Piezotronics' 484B06 signal conditioner was acquired since it had both capabilities of being AC-coupling and DC-coupling capabilities, and system has a DTC greater than 2000 seconds. The discharge time constant is appropriate for the considered solid and hybrid motor tests since the signal

decay during a single test will be less than 0.25% if most solid and hybrid motors of this size fires for 5 seconds. The chosen signal conditioner was used in the DC-coupling to avoid further *DTC* to the DAQ system and connected to a National Instruments (NI) I/O connector block, NI CB-68LP which was then wired to the USB DAQ device, NI USB-6251. After, preliminary testing a grounding issue was found and solved by adding a 5kOhm resistor to the I/O connector block. Figure 3.5 shows the DAQ hardware and sensor package. All equipment shown in Figure 3.5 was connected with the appropriate shielded cabling and connected to an MSU lab computer as shown in Figure 3.6.

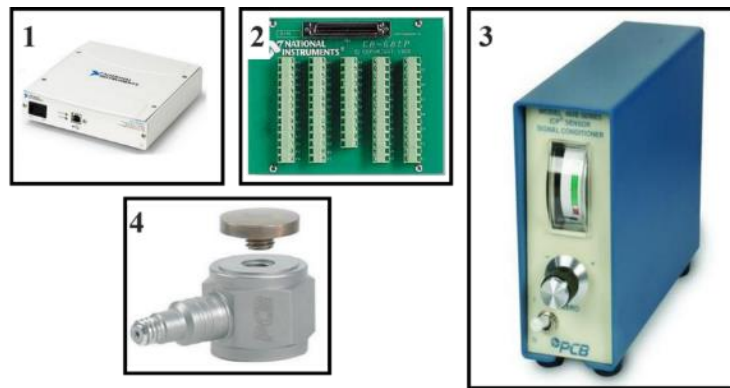


Figure 3.5 DAQ Hardware and Sensor Package

Notes: 1 – USB DAQ system [18], 2 – I/O Connector Block [19], 3 – Signal Conditioner [20], 4 – Force Sensor [17]

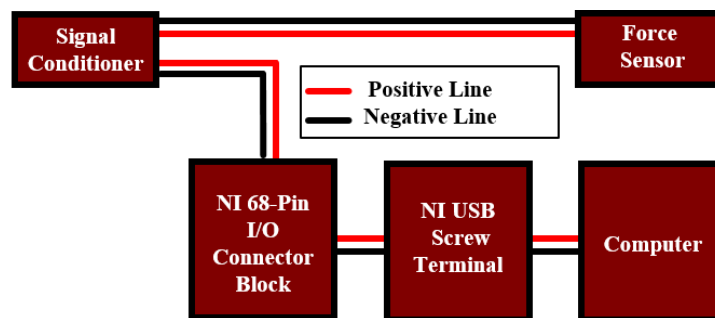


Figure 3.6 Functional Block Diagram

3.3.2 DAQ Software

LabVIEW 2016 was used to ensure all hardware would communicate properly and data acquisition transpired. To do so the 2009 Thrust Acquisition Program (TAP) was used to record and save the voltages sent by the force sensor into a comma separated value (CSV) file. The program only requires an input sample frequency which was left at 1000 Hz for all test fires and only outputs the voltage which can be later converted into pounds-force.

TAP contains three frames inside the LabVIEW program's block diagram: the first frame initializes the array for the voltage from the load cell, the second frame uses the DAQ Assistant function to continuously read the differential voltage from the load cell and creates the front panel, and the third frame stores and writes the voltages onto CSV file. Figure 3.7 shows the three frames inside the block diagram. The front panel of TAP allows the input of the desired sampling rate and view the voltage data live for preloading purposes and during testing. Once the voltage data has been collected, the stop button, shown in Figure 3.8, stops the data acquisition and allows the user to save the voltage data. [16]

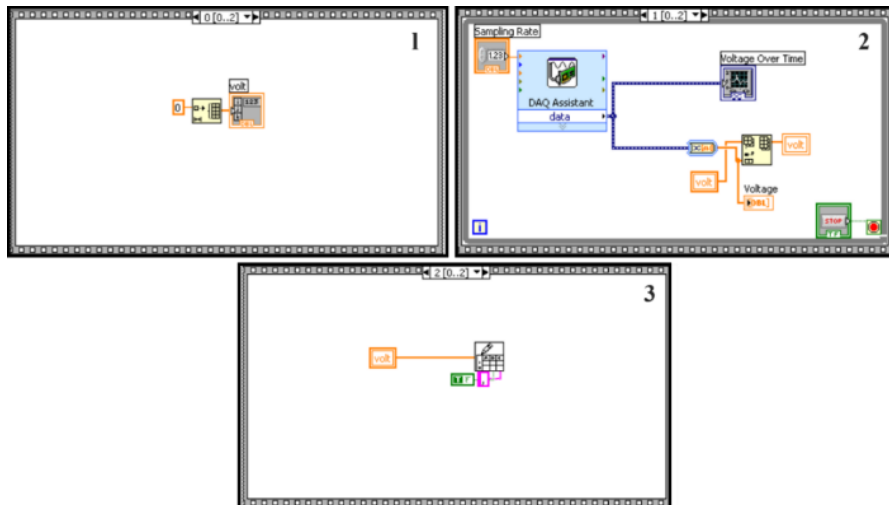


Figure 3.7 Block Diagram of Thrust Acquisition Program

Note: Figure from reference [16]

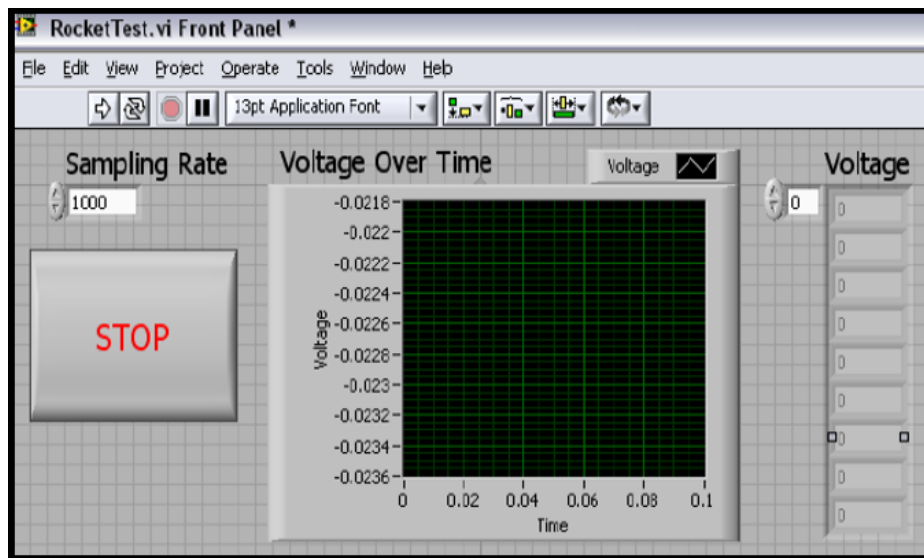


Figure 3.8 Front Panel of the Thrust Acquisition Program

Note: Figure from reference [16]

3.4 Solid and Hybrid Test Procedures

Once the ground support systems were updated, a set of solid/hybrid test fire procedures were developed which can be seen in Appendix B. All solid/hybrid tests were

performed at Mississippi State University using the commercially available hardware, MSHVTS, oxidizer flow control system, and the data acquisition system. To ensure the motor's thrust force was equally distributed to the force sensor, an aluminum cap with the same surface area as the load cell was attached to the forward section of the motor casing. Four ratchet straps were also attached to MSHVTS's structure and to the concrete ground support so no unwanted movement would be present in the system. After a failure in one of the hybrid test fires, the ratchet straps were later protected with ablative PVC insulation and Nomex material to mitigate damage.

CHAPTER IV

CHEMICAL EQUILIBRIUM WITH APPLICATION ANALYSIS

4.1 Introduction to CEA

Chemical Equilibrium with Applications (CEA) is a NASA Graphical User Interface (GUI) program that can determine chemical equilibrium compositions and properties of complex mixtures. The program's architecture is based on the Gordon and McBride assumptions and calculations to determine: the conditions for chemical equilibrium, rocket performance, shocks, and detonations. To help with these calculations, CEA includes thermodynamic and thermal transport property libraries [21]. CEA can be used to compare solid, liquid, and hybrid fuels performance.

4.1.1 Program Input

CEA is divided into three primary sections: problem, reactant, and output. Also, CEA is divided into three secondary sections: only, omit, and insert. Two of the secondary or minor sections, only and omit, do not have to be used for CEA to run, but they allow the user to select specific chemical species to be considered exclusively or omitted from the calculation. If convergence does not occur, then the user can insert possible condensed chemical species to aid in the convergence process. For the program to run successfully, the three primary sections need to be completed before the program's input file is finished.

4.1.1.1 Problem Section

To create the input file, the type of problem must be defined in CEA. CEA offers multiple types of problems including: assigned temperature and pressure, combustion (enthalpy and pressure), assigned temperature and volume, combustion (internal energy and volume), rocket, shock tube, shock, Chapman-Jouquet detonation, assigned entropy and pressure, and assigned entropy and volume. The combustion (enthalpy and pressure), hp, and the rocket, rkt, problem types were used to characterize the performance for considered propellants. As seen in Figure 4.1, these problem types can be selected, as well as, how the user wants the oxidizer and fuel (O/F) ratio to be handled. Only the O/F weight ratio was used.

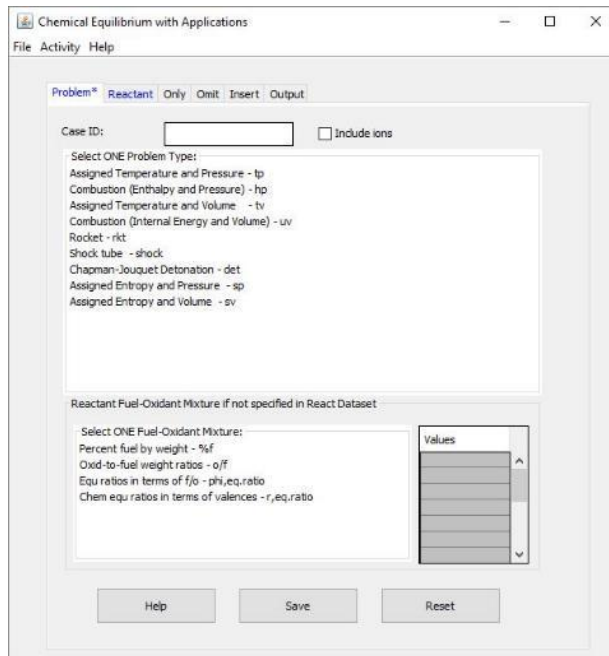


Figure 4.1 CEA Problem Selection Screen With Oxidizer Dataset

Once the problem is defined, another window will open referencing the selected problem. For the hp case, the user only has to input a range of pressures in the given units of bar, atm, psia, or mmhg. The hp case also allows inputs of an estimated temperature and an assigned enthalpy to determine if these values are used to facilitate convergence. These optional conditions were not used since the study at hand is observing generic combinations of fuels and oxidizers and these values were not known. Figure 4.2 represents the hp window described above.

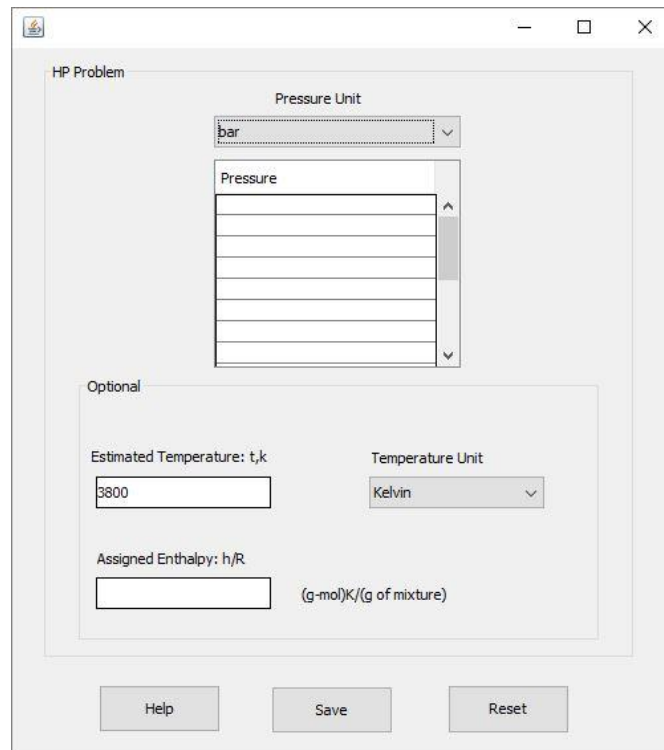


Figure 4.2 CEA Hp Case

The rkt problem expands more of what the hp problem accomplishes by adding the nozzle and chamber conditions. To redefine a new problem, the user simply selects the

reset button shown in Figure 4.1. After this is completed, the screen will be wiped clean of all work and the user can now select a new problem. Once cleared, the rkt problem can now be selected allowing a new window to appear, as shown in Figure 4.3. This window allows the user to input a range of pressures, combustion chamber characteristics, and exit conditions. The primary difference between hp and rkt problems is the new addition of the combustion chamber. This part of the program follows the Gordon and McBride rocket performance calculations at the injector, combustion chamber, nozzle, and exit. The user can define an infinite area combustion chamber that can be at equilibrium and/or if it's frozen at the combustor, throat, or the exit. The user can also define a finite area combustion chamber inputting the contraction ratio or the mass flow rate per chamber area. Only the finite area conditions were used. The optional conditions contain user assigned enthalpy, combustion temperature, and exit conditions. The user assigned enthalpy and combustion temperature was neglected, but the exit conditions were used. The exit conditions allow the user to select a range of initial and exit pressure ratios (P_i/P_e), subsonic exit and throat areas (A_e/A_t), and supersonic A_e/A_t . Figure 4.3 represents the rocket problem window described above.

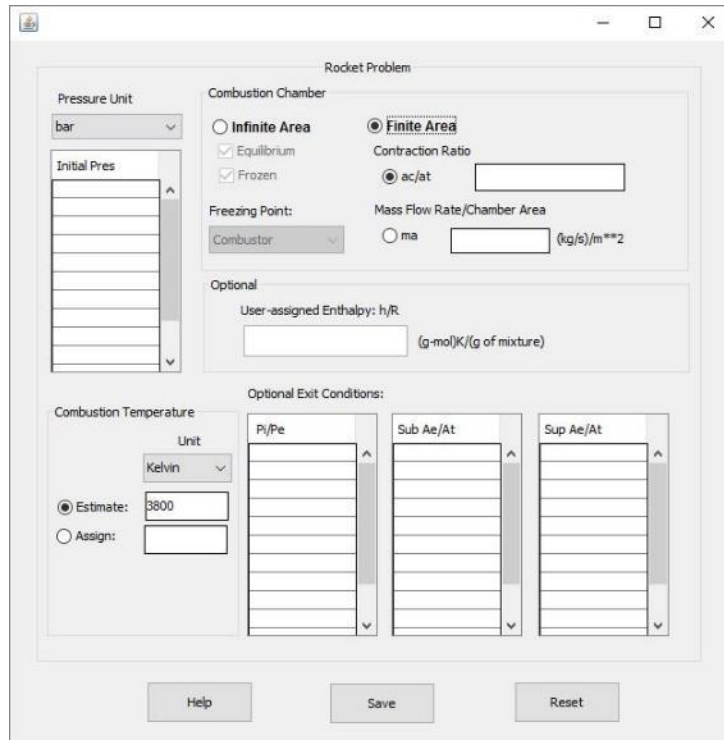


Figure 4.3 CEA Rocket Problem Window

4.1.1.2 Reactant Section

After the any problem is defined, the reactants must now be defined in CEA. CEA has a wide variety of potential reactants that the user can select from its thermodynamic library. To enter a built-in reactant into the interface, the user must first select if the substance is an oxidizer or a fuel from the “Ident” column shown in Figure 4.4. Next, the user is required to select a row in “Name” column. A new window appears and the reactant can now be chosen from an interactive periodic table database, as shown in Figure 4.5. Finally, under the “Amount” and “Temperature”, a relative weight amount or a mole amount and a reference temperature are required to be inputted.

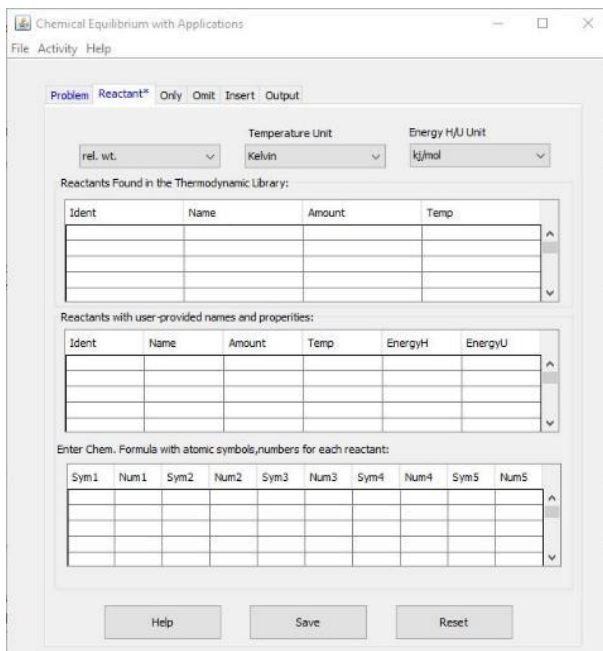


Figure 4.4 CEA Reactant Window

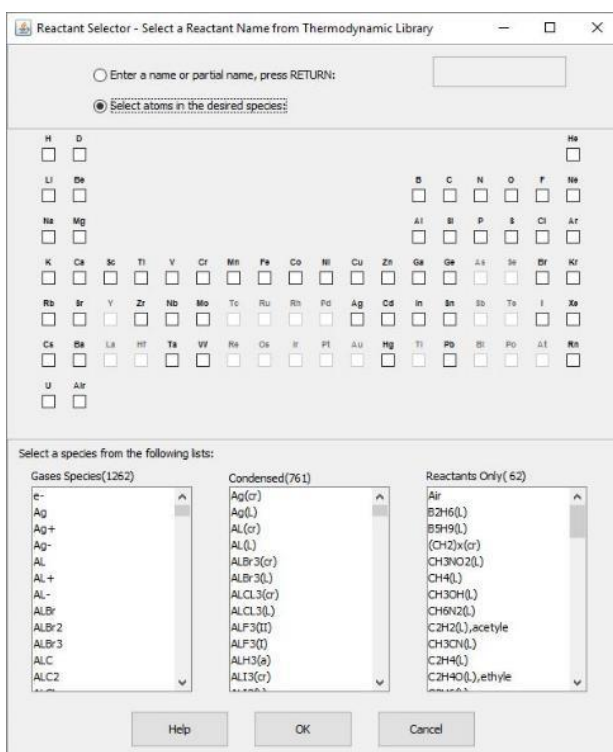


Figure 4.5 CEA Reactant Selector Window

If a reactant is not in the database, the user can define it manually into the second and third tables, as shown in Figure 4.4. The reactant will be entered normally, containing an identity, reference amount, and reference temperature; however, the user will be required to define a custom name for the chemical species, the heat of formation or the internal energy of the reactant, and the chemical structure of the reactant. Both the built-in and user defined reactants were used in this study and will be explicitly explained.

4.1.1.3 Output

The last section, output, formats the results of CEA. When running any problem type of CEA, the output tab does not change. It allows the user to customize the output file and plot file for their specific case. The output file shows all thermodynamic results, as well as the chemical composition of the products. The output file can be shortened to not show the iteration process or lengthened to show every detail in the calculation. The plot file summarizes the output file, and arranges each user selected variable into columns so it can easily be plotted in Microsoft Excel. Figure 4.6 shows the output window with no current selections.

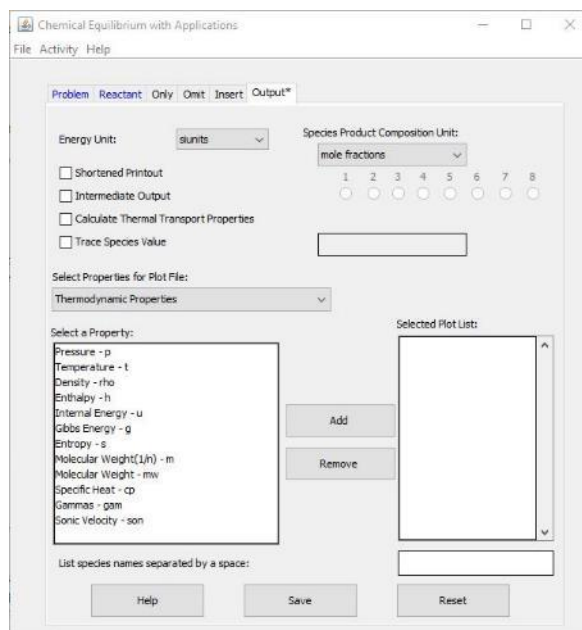


Figure 4.6 Output Window

4.2 Heat of Formation

As previously stated, either the heat of formation, ΔH_f , or the internal energy, ΔU , is required to run any CEA simulation. When discussing the energy of a molecular substance, most resources provide the heat of formation, but not internal energy; therefore, heat of formation will be used. Heat of formation, or standard enthalpy of formation, is a measure of the energy consumed or released when one mole of a substance is created under standard atmospheric conditions from its pure elements [22].

4.2.1 Group Addition Method

The heat of formation of many common compounds are known through experimentation or calculation. These heats of formations can be found in various sources such as the National Institute of Standards and Technology's (NIST) database or the

Polymer handbook [23] [24]. However, for complex structures with little known data about them, the heat of formation must be estimated. One method to do this is by the group addition method. One of the first and is most popular forms of this method was developed by Van Krevelen and Chermin, shown in equation 4.1. This method defines ΔG_f° as the free enthalpy (heat) of formation, R as the gas constant, T as the temperature, and σ as the degree of symmetry correction of the molecule [25].

$$\Delta G_f^\circ = \sum \text{contributions of component groups} + \sum \text{structural corrections} + R \cdot T \cdot \ln(\sigma) \quad (4.1)$$

Van Krevelen and Chermin later reduced this equation to:

$$\Delta G_f^\circ = \sum \text{contributions of component groups} + \sum \text{structural corrections} \quad (4.2)$$

Equation 4.2 includes equation 4.1's last term inside the structural corrections summation. This reduced equation was then assumed to consist of linear functions of temperature shown in equations 4.3 and 4.4 where the enthalpy and entropy coefficients can be seen in Table 4.1 [26].

$$\Delta G_{f,group}^\circ = \sum_{i=0}^n (A_i + B_i \cdot T_i) \quad (4.3)$$

$$\Delta G_{f,corrections}^\circ = \sum_{j=0}^n (a_j + b_j \cdot T_j) \quad (4.4)$$

Table 4.1 Enthalpy and Entropy Coefficients

Coefficient	Meaning
A_i	Enthalpy of polymerization for group contributions
B_i	Entropy of polymerization for group contributions
a_j	Enthalpy of polymerization for structural corrections
b_j	Entropy of polymerization for structural corrections

These two equations can then can be written as:

$$\Delta G_f^\circ = \sum_{i=0}^n (A_i + B_i \cdot T_i) + \sum_{j=0}^n (a_j + b_j \cdot T_j) \quad (4.5)$$

and can be reduced to equation 4.6 if the structural corrections are ignored.

$$\Delta G_f^\circ = \sum_{i=0}^n (A_i + B_i \cdot T_i) \quad (4.6)$$

When compared to the Gibbs's free energy equation, equation 4.7 and T can be assumed to be in the range of 300K-600K. [26]

$$\Delta G = \Delta H - \Delta S \cdot T \quad (4.7)$$

Equation 4.6 is an approximation since complex molecules required specific structural corrections that may not be known for a particular compound. The simplicity of the equation outweighs its approximate nature and allows it to be a useful expression. A list of small molecules and related group contributions to the heat of formation of large molecules can be seen in Appendix C.

4.3 Propellant Types

Multiple fuel types were examined with the program CEA to determine the chemical performance characteristics with varied oxidizer to fuel (O/F) ratios. Sorbitol, poly(methyl methacrylate) (PMMA), polybutadiene acrylic acid acrylonitrile (PBAN), paraffin wax, and ABS plastic were chosen in the CEA calculations as the fuel types because of their cost, availability as household goods, and historic use as hybrids. The oxidizer was always nitrous oxide, N_2O . For each of these reactants, the chemical structure, initial amount, initial temperature, and heat of formation are needed for CEA. These properties and the method by which they are input will next be described.

4.3.1 Nitrous Oxide

CEA has a wide variety of potential oxidizers that the user can select from its vast thermodynamic library. The library includes but is not limited to: liquid oxygen, nitric oxide, nitrogen dioxide, nitrous oxide, dinitrogen tetroxide, red fuming nitric acid, and many more. As previously stated, the oxidizer chosen was nitrous oxide, N_2O , due to its availability, cost, and easy to maintain.

The input values for N_2O for all cases were a relative weight amount of 100 and a reference temperature of 298.15 K. With these values CEA reported N_2O 's heat of formation to be 81.6 kJ/mol which is very close to the National Institute of Standards and Technology's (NIST) heat of formation of 82.5 kJ/mol. [27]

4.3.2 Sorbitol

Sorbitol, a sugar, is similar in appearance and physical characteristics to both sucrose and dextrose, but is classified as a hexahydric alcohol, or an "alcohol sugar" [28]. Sorbitol is found in nature in various fruits and berries, but can be made by the decomposition of dextrose [29]. Figure 4.7 represents sorbitol's chemical structure. Each vertex represents a carbon.

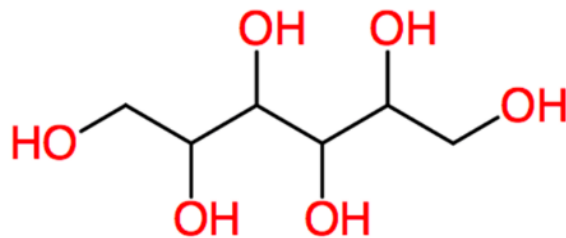


Figure 4.7 Sorbitol's Chemical Structure $C_6H_{14}O_6$

Since sorbitol was not found in CEA's thermodynamic data base, the substance was defined manually in the user-provided reactant section. The chemical formula was obtained from NIST's database and the heat of formation was found to be -1353.7 kJ/mol [30].

4.3.3 Poly(methyl methacrylate) (PMMA)

PMMA is a thermoplastic and is soft and malleable when heated and hard when cooled. It is commonly known as Plexiglas and has been used as a hybrid rocket fuel. PMMA is created synthetically from the monomer methyl methacrylate where the structure is a polymer. Figure 4.8 depicts PMMA's chemical structure. PMMA consists of an "n" identical, repeating subunits. The smallest repeating unit of PMMA is found within the brackets.

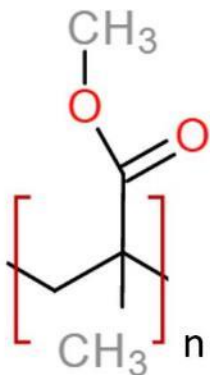


Figure 4.8 PMMA's Chemical Structure. $(C_5O_2H_8)_n$

Starting from the top CH₃ and working down, the first carbon is single-bonded to an oxygen. This oxygen is bonded to another carbon, which is also double bonded to another oxygen. That same carbon is also single bonded to another carbon, which is located in the 4-line junction towards the bottom. That carbon is bonded to two other carbons in addition to the one connected to the oxygens.

Since PMMA's heat of formation was not included in the CEA's database, and no official source has documented it, the group addition method was implemented to estimate

the heat of formation. PMMA's structure was broken down by the types of bonds that are present in a single molecule of PMMA, $n=1$. Next, using reference [31] the equations for the bond energies were found and then calculated at standard temperature and pressure. CEA reported the heat of formation of -184.48 kJ/mol Table 4.2 summarizes these calculations.

Table 4.2 PMMA Heat of Formation Calculations

Number of Bonds	Type of Bonds	Equation (J/mol)	Heat of Formation (kJ/mol)
1	- C -	1 x (20,000 +140T)	61.72
1	- O -	1 x (120,000 +70T)	-99.14
1	C=O	1 x (132,000 +40T)	-120.08
1	CH ₂	1 x (-22,000 +102T)	8.40
2	CH ₃	2 x (-46,000 +95T)	-35.38
Total Heat of Formation, (kJ/mol)			-184.48

4.3.4 Polybutadiene Acrylic Acid Acrylonitrile (PBAN)

Used as the binder for most composite propellants such as TP-H-1011, the space shuttle solid rocket boosters, PBAN can also be used as a hybrid rocket fuel on its own. Initially, the company Thiokol investigated whether liquid polybutadiene polymers could replace the current standard of polysulfide to increase the performance. In doing so, they developed a copolymer of butadiene and acrylic acid, PBAA; however, it was found to have poor tear strength. This was later changed to include acrylonitrile, which formed what today is known as PBAN [32]. Contrail Rockets, a hobby hybrid rocket company, uses similar formulations of PBAN in their hybrid fuel grains. When PBAN is used as a binder, it does give a slightly higher specific impulse, density, and burn rate than equivalent formulations using HTPB, a similar binder [33]. Chemically, PBAN is a copolymer of

butadiene, acrylonitrile, and acrylic acid, which allows this polymer to have a wide range of heats of formation depending on the relative amounts of each major ingredient. Figure 4.9 shows the chemical structure of PBAN.

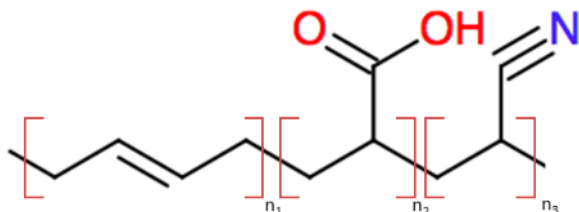


Figure 4.9 PBAN Chemical Structure, C₁₀H₁₃NO₂

Notes: In the n₁ bracket (polybutadiene), there are four carbons. The second and third carbons in the n₁ bracket are double bonded together. In the n₂ bracket (acrylic acid), there are three carbons. There are two in the lower half of the n₂ bracket, and then the third carbon is connected to two oxygens. In the n₃ bracket (acrylonitrile), there are three carbons. Two of the carbons are in the lower half of the bracket. The third carbon is in the top half of the n₃ bracket, and it is triple bonded to a nitrogen.

Since PBAN has primarily been used as a binder, little information is known about the heat of formation. However, the heat of formation could be found using the group addition method. Further research did discover the heat of formation was found to 6544.81 kJ/mol with the chemical formula to be C₆₅₄H₈₄₈N₈₉O₄ from the program PropPep3, based on an early Lockheed Martian program that calculated the propellant performance [34]. It was chosen not to calculate the heat of formation by group addition method since this PropPe3 source is reliable and the heat of formation would have been an approximation.

4.3.5 Paraffin Wax

One of the primary components of a household candle is paraffin wax, a white malleable odorless substance that can be derived from petroleum. Paraffin consists of primarily of carbon and hydrogen atoms classifying it as a hydrocarbon. Specifically in chemistry, paraffin is also known as an alkane due to its chemical structure of C_nH_{2n+2} . Paraffin's chemical can structure vary depending on how many molecules of carbon and hydrogen it contains. However, in the case for paraffin the chemical structure is C_nH_{n+2} where n is from 19 to 36 [14]. For instance, methane (CH_4) is an alkane because it has the structure of C_nH_{2n+2} , but since n is equal to one methane is not a paraffin. Since for any given paraffin, the number of n can vary, an averaged value off $n = 25$ was used since very little data is known. Figure 4.10 shows the chemical structure of paraffin wax with n equal to 25.

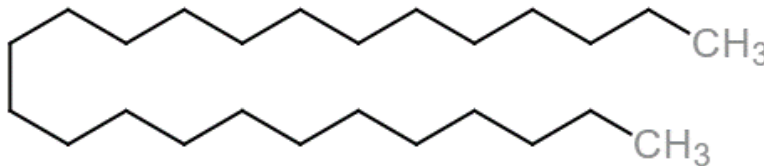


Figure 4.10 Paraffin Wax Chemical Structure $C_{25}H_{52}$

To estimate the heat of formation of paraffin, it was calculated by using the heat addition method. Paraffin's chemical formula was broken down to CH_2 and CH_3 bonds. This breakdown becomes



where CH₂'s heat of formation contribution depends on the n value. Figure 4.11 shows the generic structure of paraffin wax.

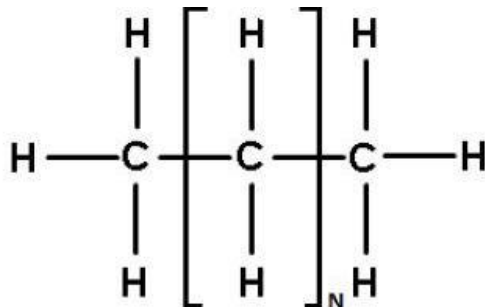
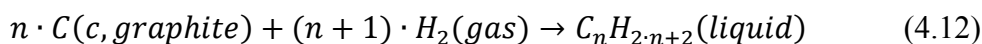
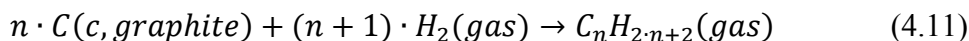
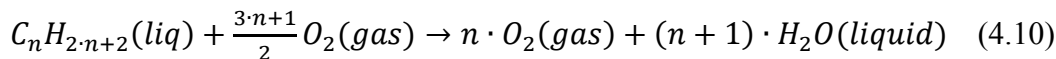
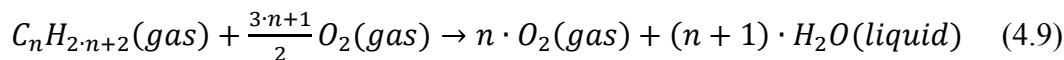


Figure 4.11 Paraffin's Generic Chemical Structure, C_nH_{2n+2}

Since the chemical structure of the paraffin contained multiple bonds, it was decided not to use bond energy calculations to find the heat of formation, but to obtain a more precise heat of formation for paraffin by using experimental data. The resource material used experimental values of several forms of paraffin to obtain the heat of formation and combustion of paraffin at any n value. First, balanced chemical equations, equation 4.9 through 4.12, were written in terms of n so an iteration process could be formed to find the heat of formation and combustion of paraffin in gas and liquid form [35].



These equations were then evaluated with experimental data [35] and to give the heat of formation in equations 4.13 through 4.16 with their corresponding uncertainty values.

$$\Delta H_{combustion(gas)} = (57.909 + 157.443 \cdot n) \frac{kcal}{mol} \quad (4.13)$$

$$\Delta H_{combustion(liquid)} = (57.430 + 156.263 \cdot n) \frac{kcal}{mol} \quad (4.14)$$

$$\Delta H_{formation(gas)} = (-10.887 - 4.926 \cdot n) \frac{kcal}{mol} \quad (4.15)$$

$$\Delta H_{formaiton(gas)} = (-10.887 - 6.106 \cdot n) \frac{kcal}{mol} \quad (4.16)$$

Finally, the heat of formation was calculated at n values of 15, 20, and 25 as shown in Table 4.3. Appendix D shows the heat of formation of paraffin calculations including the heat of combustion calculations.

Table 4.3 Heat of Formation of Paraffin Wax C_nH_{2n+2}

"n" Value	Heat of Formation, Gas (kJ/mol)	Heat of Formation, Liquid (kJ/mol)
15	-352.94	-429.05
20	-456.06	-556.87
25	-559.18	-684.70

Since paraffin will be in both liquid and gaseous states during combustion, average values for n = 25 giving -621.94 kJ/mol were chosen. This compares favorably to other sources such as [36] where $\Delta H = -598$ kJ/mol where n = 23.

4.3.6 Acrylonitrile Butadiene Styrene (ABS)

The final fuel to be discussed is ABS plastic. ABS is classified as a thermoplastic polymer due its moldable nature. This characteristic allows it to be used in many applications such as appliances, toys, household piping, automotive components, and 3D

printing [37]. Chemically, this plastic is comprised of three monomers: acrylonitrile, 1,3 butadiene, and styrene to create the terpolymer, a copolymer consisting of three monomers [38]. Acrylonitrile, 1,3 butadiene, and styrene monomer chemical structures can be seen in Figure 4.12

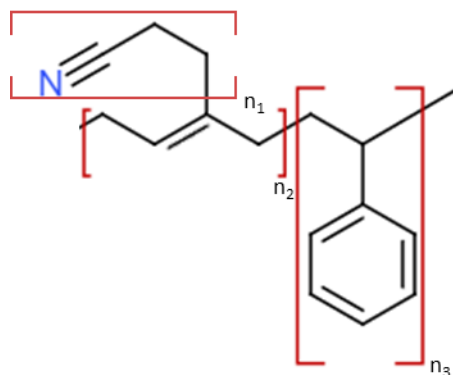


Figure 4.12 ABS Chemical Structure, $(C_3H_3N C_4H_6 C_8H_8)_n$

Notes: Starting from the n_1 bracket is acrylonitrile (C_3H_3N) where there are three carbons. A carbon is triple bonded to a nitrogen and then single bonded to a carbon. This carbon is single bonded to two hydrogens and another carbon atom. This carbon is then bonded to the n_2 bracket which is butadiene 1,3 (C_4H_6). Butadiene 1,3 contains a chain of four carbons to of which are double bonded. One carbon, as previously discussed, attaches to the acrylonitrile while another attaches to the styrene, n_3 bracket. Styrene (C_8H_8) contains eight carbons and hydrogens; six of each are in a benzene ring structure (C_6H_6).

Due to ABS's complex chemical structure, the group addition method must be used to estimate the heat of formation. To do so the following information is required: heat of formation of the monomer, $\Delta H_{f,monomer}$, heat of formation of polymerization, $\Delta H_{f,polymerization}$, heat of formation of the polymer, $\Delta H_{f,polymer}$, and the mole fraction of each monomer. $\Delta H_{f,monomer}$ and $\Delta H_{f,polymerization}$ values were found using the NIST website [23] and the polymer handbook [24], respectively. Once these values were found, $\Delta H_{f,polymer}$

was calculated by subtracting $\Delta H_{f,polymerization}$ from $\Delta H_{f,monomer}$. This principle was described by Van Krevelen and shown in equation 4.17 [26].

$$\Delta G = \Delta H - \Delta S \cdot T = G_{polymerization} - G_{monomer} \quad (4.17)$$

Next, the mole fractions were calculated from the weight percentages that were given by the manufacturer. CHEI MEI Corporation, one of the main sources for plastic and rubber material supplies in the United States, quotes the following weight percentages of their black ABS: acrylonitrile 20 – 40 %, butadiene 19 – 23 %, styrene 54 – 58 %, and additive 1 – 2 %. The data sheet appears in Appendix E [39]. The additive is more than likely the coloring of this particular ABS plastic which was neglected from these calculations. The average percentage of each monomer was taken to calculate the molar fraction of each monomer. Table 4.4 shows the mole fractions and the results of heat of formation calculations.

Table 4.4 Heat of Formation of ABS Calculation

Monomer	$\Delta H_{f,monomer}^{\circ}$ (kJ/mol)	$\Delta H_{f,polymerization}^{\circ}$ (kJ/mol)	$\Delta H_{f,polymer}^{\circ}$ (kJ/mol)	ABS Mole Fraction	$\Delta H_{f,subtotal}^{\circ}$ (kJ/mol)
Acrylonitrile	176.6 [40]	76.5 [41]	100.1	0.421	42.14
Butadiene	108.8 [42]	73.0 [41]	36.7	0.394	14.46
Styrene	146.9 [43]	74.5 [41]	62.31	0.541	33.71
$\Delta G_{f,ABS}^{\circ}$					90.312

Finally, using the mole fractions, the heat of formation and the chemical formula for ABS were found to be 90.312 kJ/mol and $C_{17.03}H_{18.9}N$ respectively. Similar ABS heat of formation calculations were performed [3], and yielded 62.62 kJ/mol and a chemical equation of $C_{8.95}H_{11.28}N$ [3]. These calculations are only different due to different source of materials and the quote on mole fractions. These differences can be seen in Table 4.5.

The chemical structure and heat of formation of all selected fuels that will be tested in CEA are summarized in 0.

Table 4.5 MSU and USU ABS Heat of Formation Calculations Comparison

Monomer	$\Delta H_{f,MSU}$ (kJ/mol)	$\Delta H_{f,[3]}$ (kJ/mol)
Acrylonitrile	42.14	42.27
Butadiene	14.46	16.0
Styrene	33.71	4.36
Total	90.31	62.63

Table 4.6 User Selected CEA Fuel Characteristic

Characteristic	Sorbitol	PMMA	PBAN	Paraffin	ABS
Heat of Formation (kJ/mol)	-1353.7	-184.48	6544.8054	-621.94	90.31
Chemical Structure	$C_6H_{14}O_6$	$C_5O_2H_8$	$C_{654}H_{848}N_{89}O_4$	$C_{25}H_{52}$	$C_{17.03}H_{18.9}N$

4.4 Similar Hybrid Studies Using CEA

CEA has been used in solid, liquid, and hybrid propulsion applications from classroom demonstrations to publications from several universities. Utah State and Stanford University papers have used the hp case and the rocket case, respectively, to gain a better understanding of the chemical reactants inside the combustion and performance characteristic of a nitrous oxide fed hybrid motor [3] [36] [44]. These references were studied, accurately reproduced, and expanded upon using the current study's findings of the five chosen fuels.

4.4.1 CEA Enthalpy and Pressure Simulations

Reference [3] approximated the heat of formation and then calculated the chemical compositions of HTPB, ABS, and paraffin, which were then entered into CEA's combustion enthalpy and pressure case to find the thermodynamic and transport properties of a hybrid motor using nitrous oxide. The computations used at pressures of 100 kPa, 500 kPa, 1500 kPa, 4000 kPa, and 75000 kPa with a range of oxidizer/fuel ratios from 1 to 11. These simulations provided the following data sets: specific heat ratio, molecular weight, characteristic exhaust velocity, adiabatic flame temperature, viscosity, and Prandtl number [3] [36]. It was decided to rerun these simulations to include O/F ratios below 1, and to only focus on the adiabatic flame temperature T_0 , specific heat ratio γ , molecular weight M_w . These runs were used to ensure validity of all future CEA runs, and to gain a better understanding how the difference of inputs, heat of formation and chemical formula, would affect the output. The reference ABS and Paraffin was rerun only. HTPB wasn't considered since PBAN is very similar HTPB. Table 4.7 reviews reference [3] as well as the current experiments inputs into CEA.

Table 4.7 Enthalpy and Pressure CEA Input

Pressure Range (kPa)	100, 500, 1500, 4000, 7500	
O/F Ratio	0.5 – 11 (increments of 0.5)	
Temperature (oxidizer and fuel) (K)	298.15	
Relative Weight Amount	100	
Oxidizer (built into CEA)	N ₂ O	
Fuel	Heat of Formation (kJ/mol)	Chemical Formula
Paraffin [3]	-598	C ₂₃ H ₄₈
ABS [3]	62.63	C _{8.955} H _{11.28} N
Paraffin	-621.94	C ₂₅ H ₅₂
ABS	90.31	C _{17.03} H _{18.903} N

Notes: Reference [3] calculated the heat of formation for a paraffin n=23, but states that n=25 was chosen. Assuming that the calculations were supposed to n=23 be for the simulations were run accordingly.

The combustion chamber pressure is not currently known for the present experiments so an estimation of 4000 kPa (580 psi) was chosen to serve as a middle ground for a comparison. Figure 4.13 - Figure 4.15 shows the reference ABS and Paraffin and the current experiments ABS and paraffin calculated in CEA at 4000 kPa.

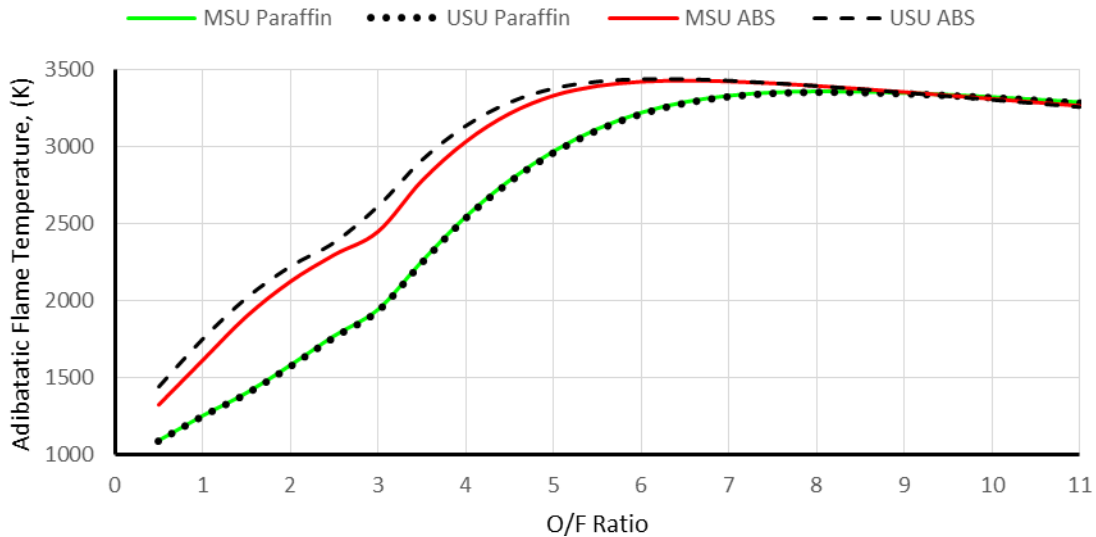


Figure 4.13 CEA Hp: Adiabatic Flame Temperature for Paraffin and ABS

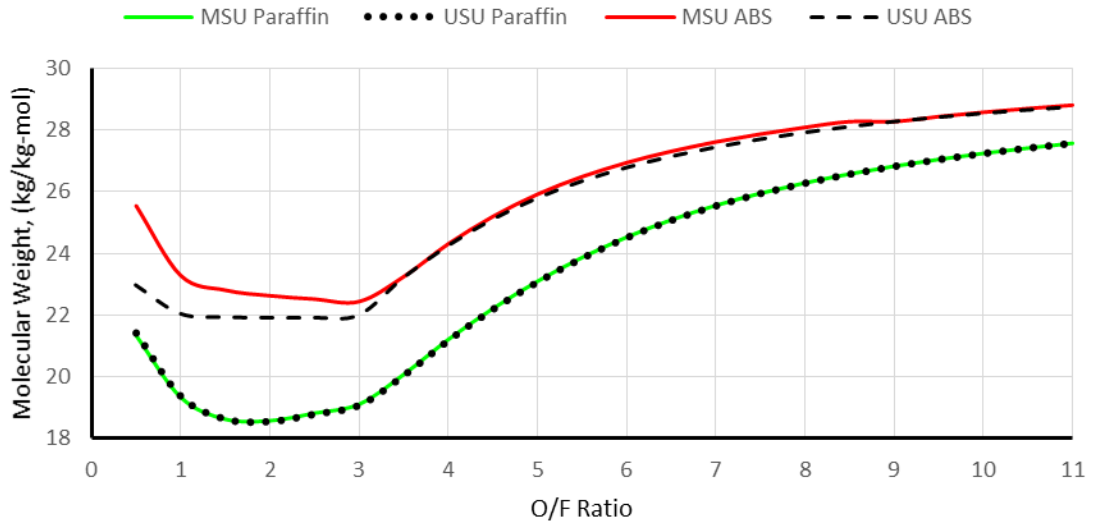


Figure 4.14 CEA Hp: Molecular Weight for Paraffin and ABS

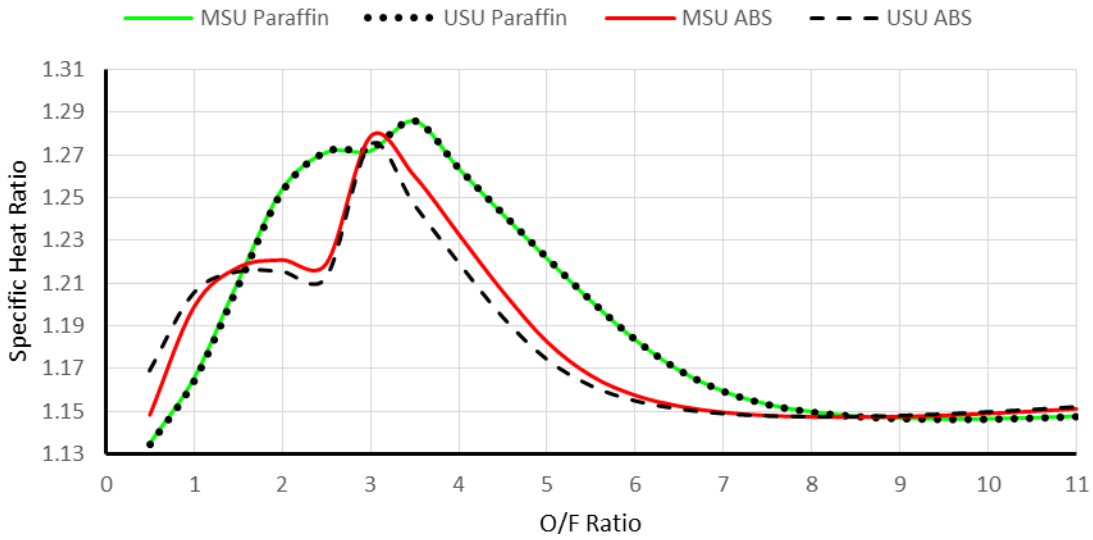


Figure 4.15 CEA Hp: Specific Heat Ratio for Paraffin and ABS

The hp CEA simulations showed some interesting results. All of reference [3] and current paraffin curves are almost identical, which means that a slight change of “n” and a higher heat of formation doesn’t affect the thermal properties that much. The changes of

the ABS is more noticeable when observing the temperature and the specific heat ratio curves. For instance, at an O/F of 3 the specific heat ratio and molecular weight are larger in the current ABS when compared to the reference ABS while the temperature is higher for the reference ABS. This information could aid propellant manufactures on how certain mixtures of fuel change the performance properties of their propellant.

4.4.2 CEA Rocket Problem Simulations

NASA Ames conducted simulations with CEA’s rocket problem simulation to characterize four specific fuels: sorbitol, HDPE, HTPB, and PMMA [44]. These simulations assumed equilibrium combustion at 500 psia and expanding to sea level conditions. NASA Ames’s atmospheric, combustion chamber, and nozzle conditions were re-simulated in CEA’s rocket problem section, but the fuels HDPE and HTPB were excluded from the analysis. The simulation did included sorbitol, PMMA, paraffin, ABS, and PBAN. The simulation’s purpose was to find the combustion chamber’s specific impulse, I_{sp} , of each of the 5 fuels at a varying O/F ratio. Table 4.8 shows the CEA inputs for this NASA Ames case and Figure 4.16 shows the results of the NASA Ames rocket problem simulation. The simulation was accurately reproduced for sorbitol, and were within tolerance of PMMA. [44]

Table 4.8 NASA Ames Rocket Problem Conditions

Initial Pressure (kPa)	A_c/A_t	P_i/P_e
3447.4	3.917	34.014

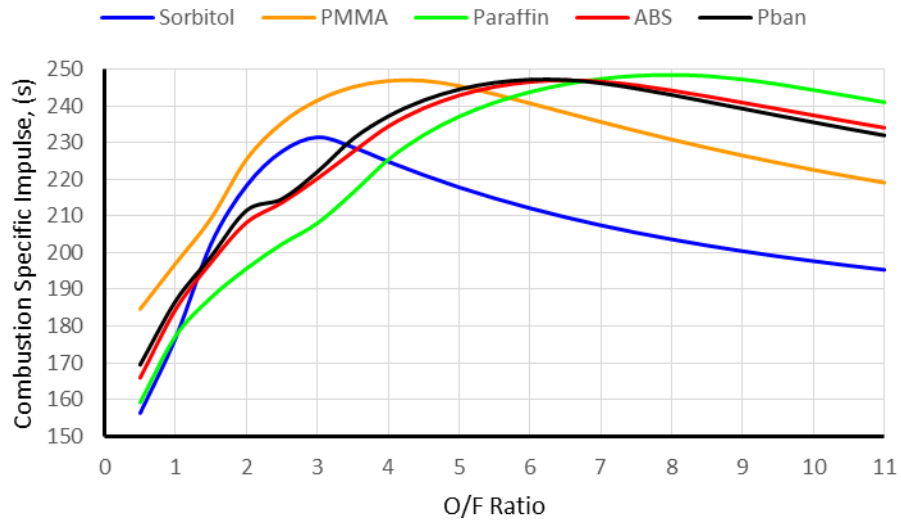


Figure 4.16 [44] Specific Impulse with Selected Fuels

This NASA Ames rocket problem simulation shows how to properly use CEA’s performance prediction while achieving some knowledge how the fuels will act in the combustion chamber. When the O/F increases the I_{sp} for each fuel increases, but then peaks and slowly decreases. Sorbitol and PMMA increase very quickly while paraffin, ABS, and PBAN increase at a slower rate but become at top off at a higher I_{sp} in the range of O/F 6 - 8.

4.5 Performance Predications

After the reference simulations concluded, simulations were ran to estimate the performance characteristics of each fuel at the conditions at which they would operate. The initial pressure was varied from 3200 kPa (464.12 psi), 4000 kPa (580.15 psi), and 4200 kPa (609.16 psi) since the pressure at the injector was estimated to be below the vapor pressure of N_2O . The nozzle’s combustion, throat, and exit areas were calculated to find A_c/A_t and A_e/A_t then were inputted into CEA shown in Table 4.9. The simulations

calculated pressure, temperature, specific impulse, specific heat ratio, and molecular weight at the combustion chamber, throat, and exit. Figure 4.17 shows the 4000 kPa exit condition results.

Table 4.9 MSU Rocket Problem

Initial Pressure (kPa)	Area of Combustion (mm ²)	Area of Throat (mm ²)	Area of Exit (mm ²)	Ac/At	Supersonic Ae/At
3200, 4000, 4200	913.92	142.33	1036.17	6.421	7.28

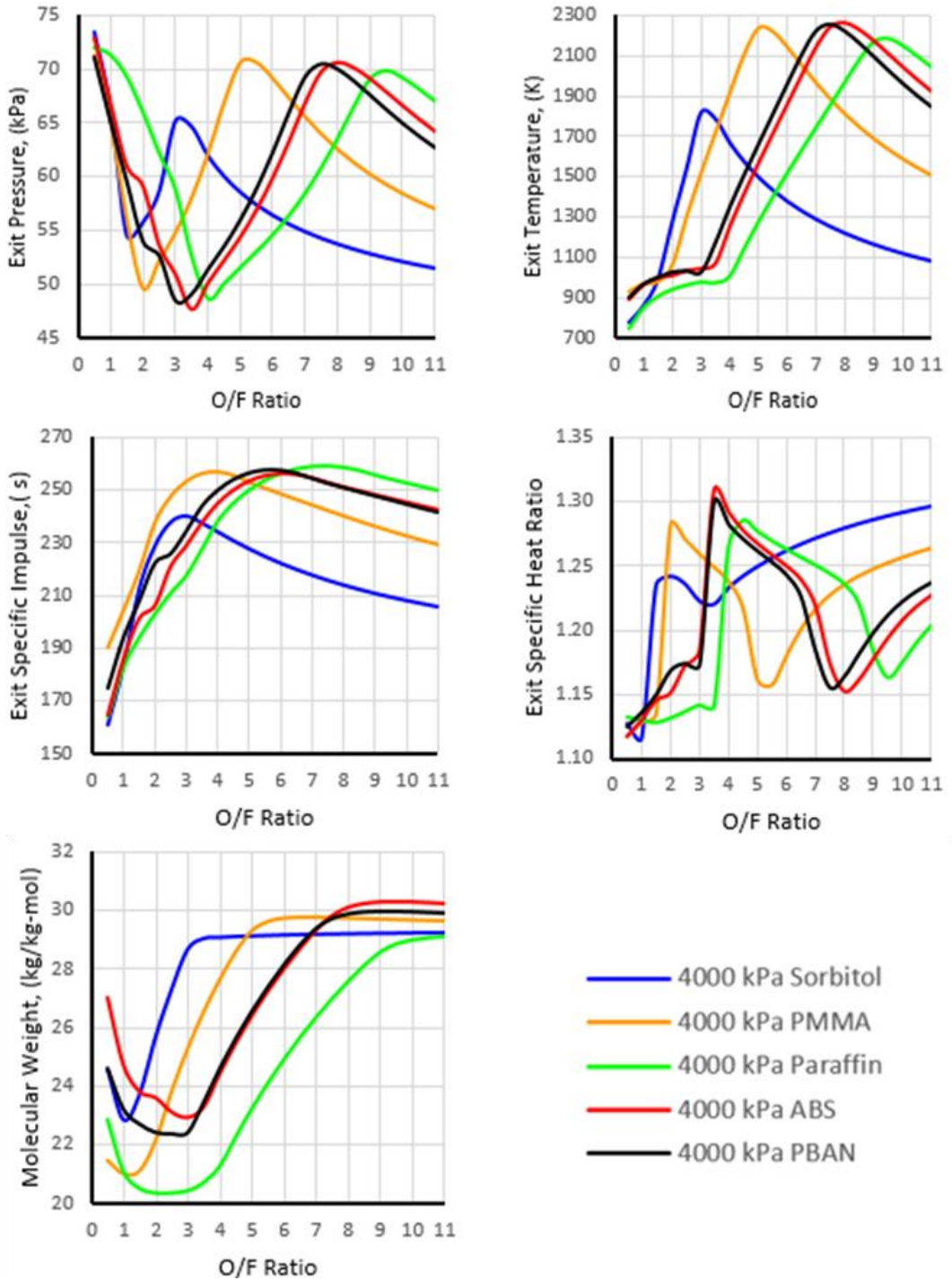


Figure 4.17 Exit Performance Conditions at 4000 kPa

These simulations gave valuable insight to how each fuel behaves at a varying O/F ratio. The simulations show that pressure, temperature, and ISP at an O/F between 3.5 and 7, PMMA, PBAN, ABS, and paraffin, increase, peak, and then decrease. PMMA does peak earlier than all three fuels followed by PBAN, ABS, and then paraffin.

CHAPTER V

TEST RESULTS

5.1 Data Extraction Software

A Mathcad code was developed to extract the thrust curve from the raw voltage data gathered from the DAQ system. The code was designed to calculate an average of the initial voltage to zero out the preloading, convert the voltage to pound-force, find the ignition time using a standard deviation function and threshold while loop, allow the user to manually set when the data set will end, and output the data into a csv file. The code can be seen in Appendix F.

5.2 Results

When analyzing the solid and hybrid test fires, measured and video data were taken and compared to understand how the fuel behaves during operation. As previously discussed, the force sensor would capture the thrust measurements for each fuel at a function of time while high definition cameras captured videos and photography images. The test fires were recorded and logged into Table 5.1.

Table 5.1 Solid/Hybrid Test Fire Log

#	Date	Propellant	Designation	Comments
1	9/26/2015	Cesaroni Solid	J760	Tested vertical stand and experimental blast deflector no data
2	11/21/2015	Cesaroni Solid	J760	Data recorded and verified
3	2/27/2016	ABS/Paraffin	Rectilinear 10% Fill (concept)	Tested nitrous system and fuel concept. System deemed safe. No data.
4	3/4/2016	ABS/Paraffin	16 Cell (concept)	Tested final configuration of test hardware and new fuel concept. No data.
5	3/4/2016	Cesaroni Solid	J760	Data recorded and verified with final test setup.
6	5/10/2016	Conrail PBAN	K-321	Data recorded.
7	5/10/2016	Conrail PBAN	K-321	Data recorded.
8	5/19/2016	Conrail PBAN	K-321 (9 inch)	Data recorded.
9	5/19/2016	Conrail PBAN	K-321 (9 inch)	Data recorded.
10	5/19/2016	ABS/Paraffin	4 Cell	Test fire success. Data failed to capture.
11	5/19/2016	ABS/Paraffin	4 Cell	Misfire. Motor tube ruptured near nozzle due to an injector failure.
12	5/28/2016	ABS/Paraffin	4 Cell	Data recorded.
13	5/28/2016	ABS/Paraffin	4 Cell	Misfire. Snap ring failure.
14	6/22/2016	ABS/Paraffin	4 Cell	Data recorded.
15	6/22/2016	ABS/Paraffin	8 Cell	Data recorded.
16	6/22/2016	ABS/Paraffin	16 Cell	Data recorded.
17	6/24/2016	ABS/Paraffin	4 Cell	Data recorded.
18	6/24/2016	ABS/Paraffin	8 Cell	Misfire. Snap ring failure.
19	6/28/2016	ABS/Paraffin	8 Cell	Misfire. Motor tube failed towards nitrous vent.
20	9/11/2016	Cesaroni Solid	J760	Updated test stand and verified. Data recorded.
21	9/22/2016	ABS/Paraffin	16 Cell	Success
22	9/22/2016	ABS/Paraffin	16 Cell	Preloading lost due to failed ratchet straps
23	9/22/2016	ABS/Paraffin	8 Cell	Tube Failure
24	9/22/2016	ABS/Paraffin	8 Cell	Tube Failure

5.2.1 Preliminary Test Fire Results

Before testing the ABS/paraffin fuel, multiple commercially available solid and hybrid motors were test fired to verify the validity of the system and to create a baseline comparison. Cesaroni's J760 solid propellant motors were selected as the solid propellant comparison due to similar peak thrust and average thrust that was to be expected from the tested hybrid motors. Contrail's K321 PBAN hybrid motor was chosen for its nozzle and injector selection. The K321's nozzle and injector would be the exact same as the ABS/paraffin fuel. The J760's and K321's test thrust curve and manufacturer thrust curve can be seen in Figure 5.1 and Figure 5.2.

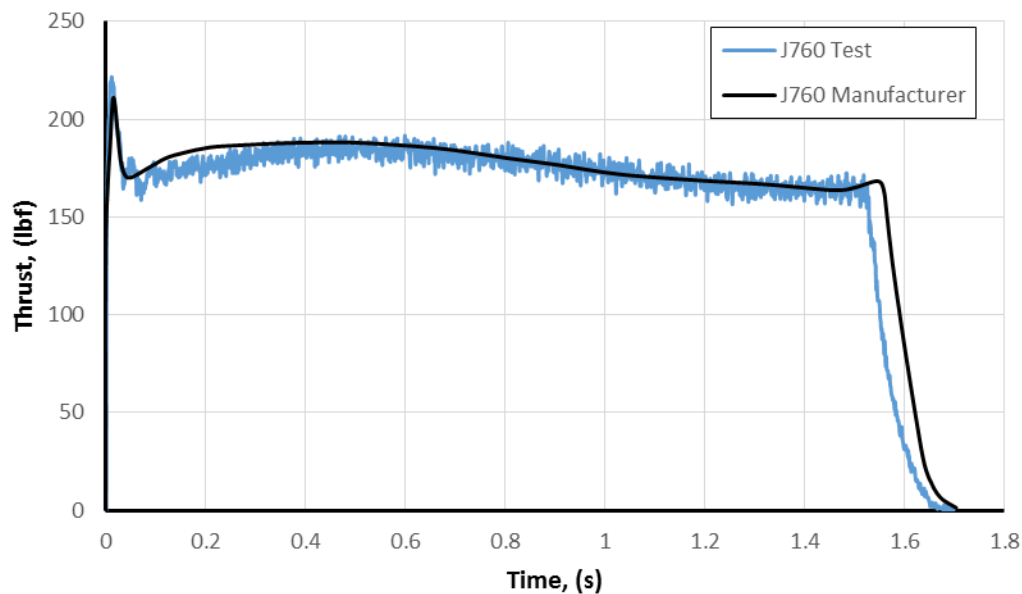


Figure 5.1 J760 Thrust Curve Comparison

Note: The manufacturer curve can be found in reference [45].

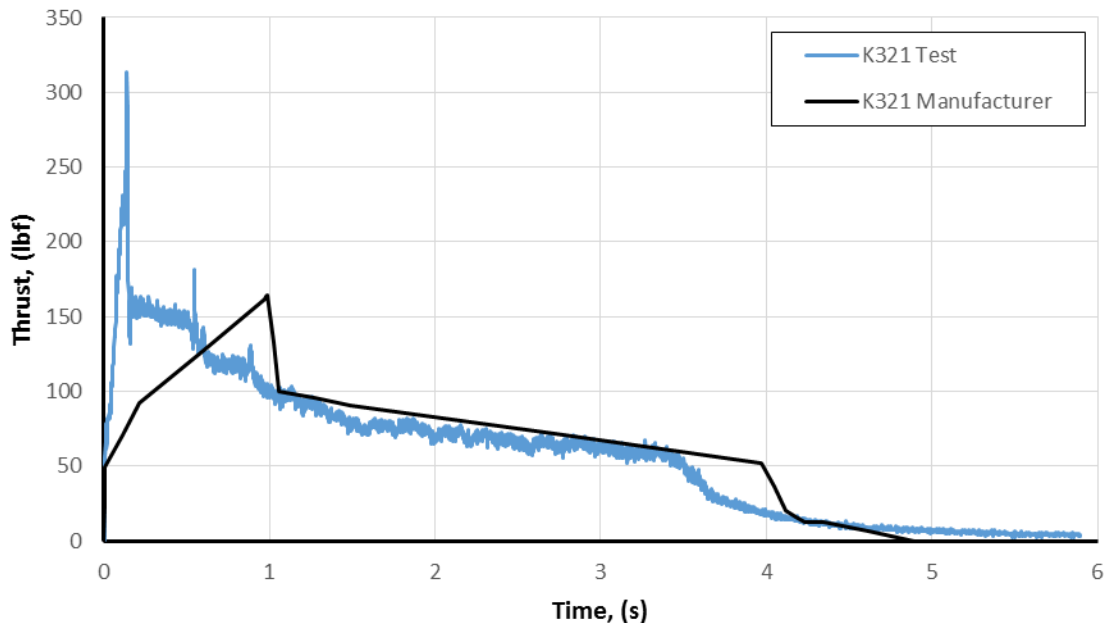


Figure 5.2 K321 Thrust Curve Comparison [46]

Figure 5.1 shows that the DAQ system and MSHVITS captured the thrust curve of the J760's shape accurately with slight differences. These differences can be attributed to differences in motor performance and small losses caused by the test stand. Repeated test fires of the J760 motors were performed and the same thrust curve was shown throughout all tests. The K321 thrust curves shown in Figure 5.2 show greater differences in regards to the basic shape and peak thrust, but the total impulse was only off by a 2% difference between the two curves. Comparing the K321 test data and the manufacturer data shows a quick rise to peak thrust for the test data while the manufacturer data shows a rate of decrease in thrust. The K321 tests were repeated, but the shape remained the same. The rate of decrease in thrust of the manufacturer's K321 curve can be attributed to how the N_2O was handled when tested for certification. Therefore, the manufacturer data was not used as a comparison for this study.

After the preliminary solid and hybrid test fires concluded, more of the same commercially available K321 PBAN grains were then reduced in length from 12 in to 9 in to compare to the ABS/paraffin fuel grains. Shown in Figure 5.3, these PBAN fuels were designated K321 Short and would be the control for future hybrid tests. Both test fire's shapes were very similar with each other with slight differences to peak thrust, 290 lbf and 226.3 lbf respectively, but total impulses were within 0.17% each other.

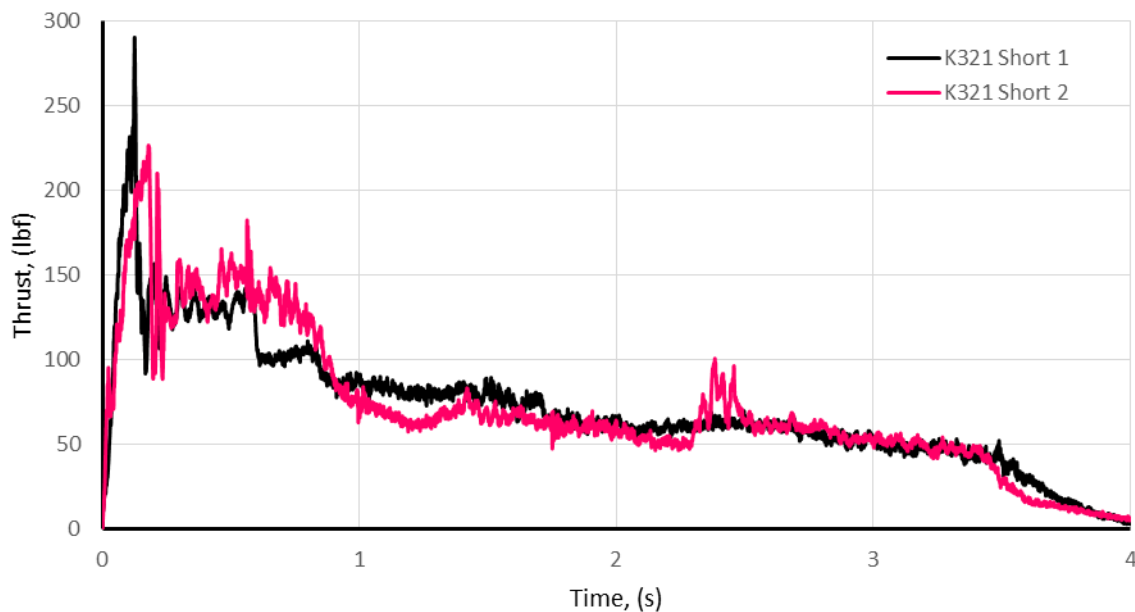


Figure 5.3 “K321 Short” Thrust Curves

5.2.2 ABS/Paraffin Test Fire Results

The four cell design was first selected to be fired due to its higher paraffin composition followed by the eight and sixteen cell designs. After the four cell fuel test fires concluded, the thrust data was found to be very noisy so a moving average of the data was

done to clean up the noise. Figure 5.4 shows the unfiltered thrust curves while Figure 5.5 shows the filtered thrust curves.

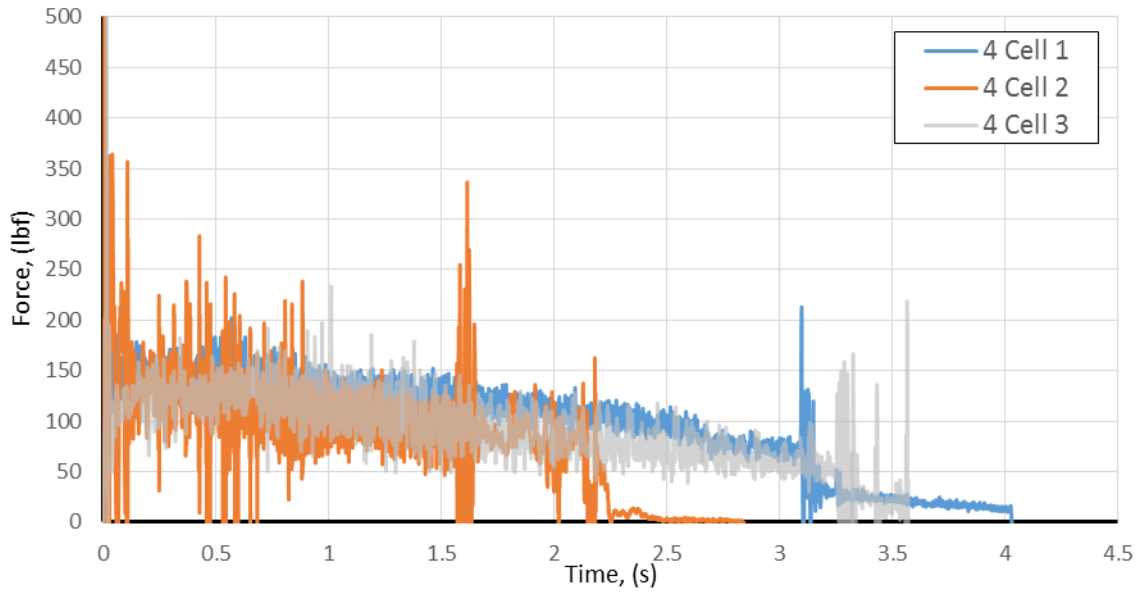


Figure 5.4 Unfiltered Four Cell Fuel Thrust Curves

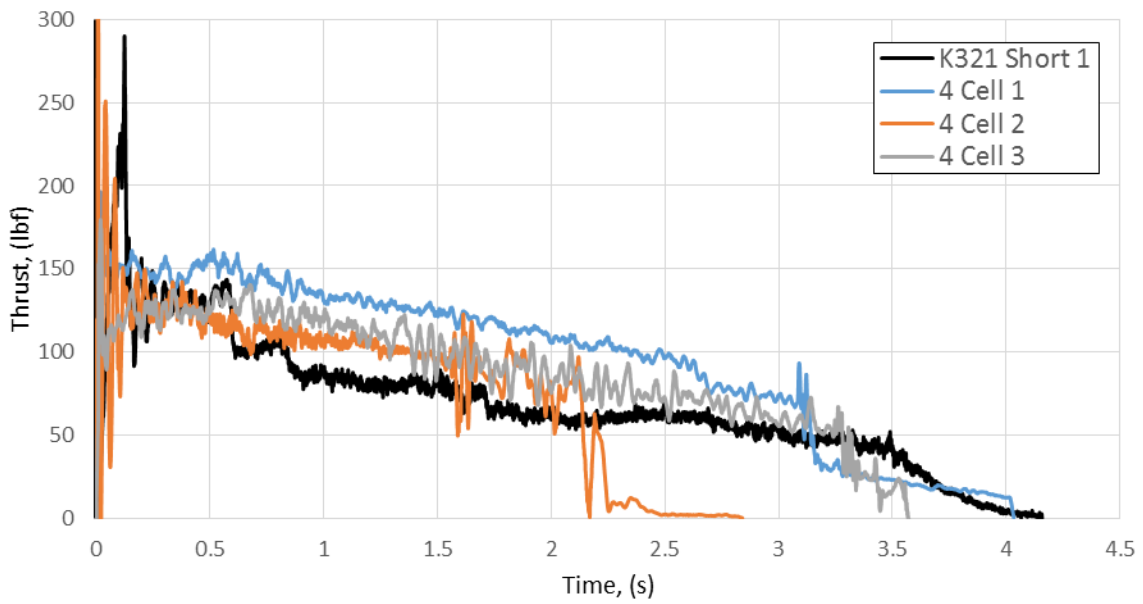


Figure 5.5 Filtered Four Cell Fuel Thrust Curves

All three four cell fuel test fires were considered a success. However, the second test fire failed to burn some of the ABS/paraffin fuel when ignited. This failure to burn could have been an improper separation and ignition of the N₂O line from the injector, or the ABS structure of the fuel failed sooner than expected.

The eight and sixteen cell test fires were then tested. Unfortunately during the beginning of the eight and sixteen test fires, several snap ring and casing failures occurred. These hardware failures ultimately stopped further testing of these two cell configurations and other planned tests such as PMMA fuel test and different ABS/paraffin fuel designs. Figure 5.6 and Figure 5.7 shows the eight and sixteen cell data.

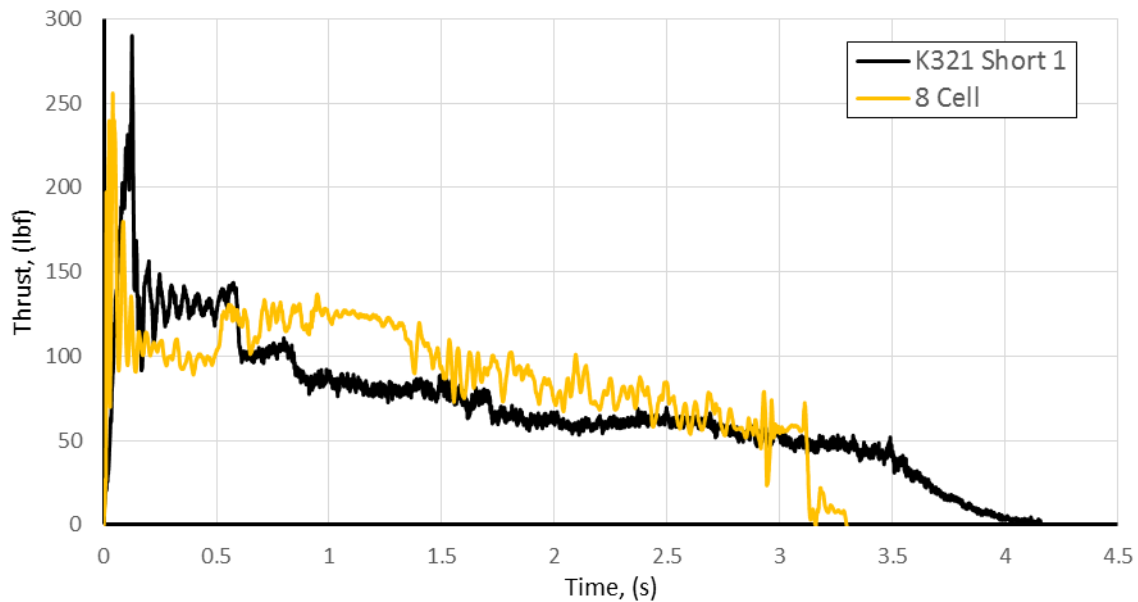


Figure 5.6 Eight Cell Filtered Thrust Curve

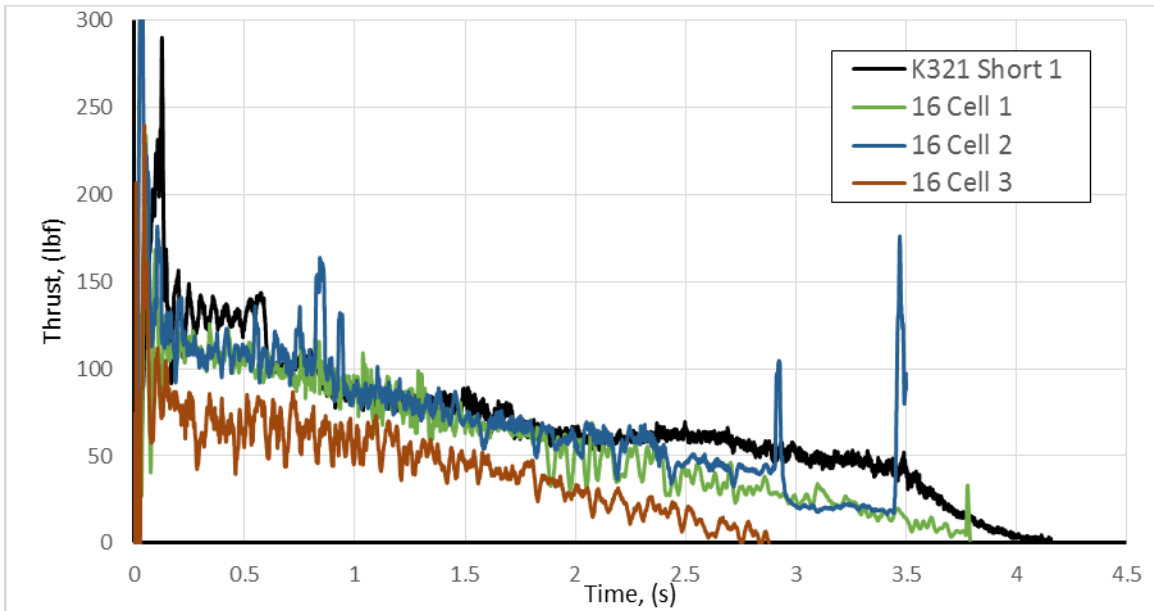


Figure 5.7 Sixteen Cell Filtered Thrust Curve

The eight cell data shown in Figure 5.6 coincides with the four cell 3 data from Figure 5.5 with respect to burn time and average thrust. The sixteen cell data has a lower overall average thrust, but consistent burn time of that of both four and eight cell geometries. The sixteen cell 2 data set stops abruptly at 3.5 seconds due to a ratchet strap failure, although the burn lasted approximately 4 seconds. The sixteen cell 3 data shows a significant decrease in burn time which was due to an incomplete burn of the ABS/paraffin fuel. Figure 5.8 shows the best test data of the four, eight, and sixteen cell geometries. The comparison shows that the four cell geometry does provide the best thrust when compared to the eight, sixteen, and K321 short test fires.

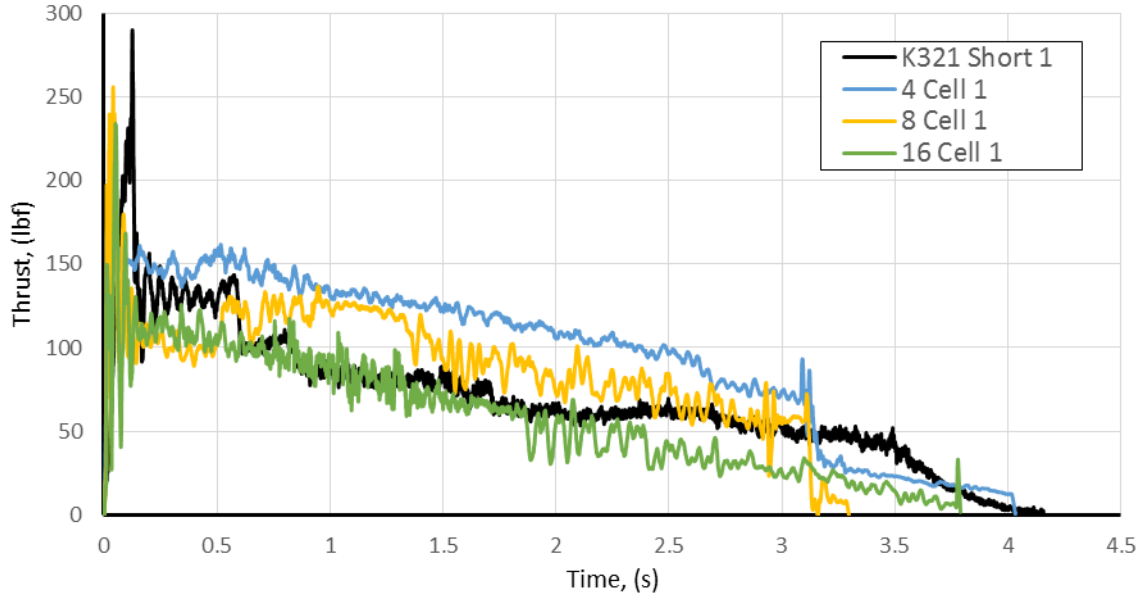


Figure 5.8 Four, Eight, Sixteen Cell Thrust Comparison

Equation 5.1 was used to find the total impulse, I , using the thrust data, F , and the change in time, Δt , of each test fire. The results were recorded in Table 5.2.

$$I = \int F dt \tag{5.1}$$

Table 5.2 Hybrid Test Results

Test Number	Motor Designation	Fuel Mass (lbm)	Peak Thrust (lbf)	Burn Time (s)	Total Impulse (lbf*s)
8	K321 Short	0.503	290	4.16	285
9	K321 Short	0.485	226	4.23	286
12	4 Cell	0.639	380	4.03	390
13	4 Cell	0.626	196	2.84	231
14	4 Cell	0.631	179	3.57	321
15	8 Cell	0.637	255	3.30	297
23	8 Cell	0.639	N/A	N/A	N/A
24	8 Cell	0.646	N/A	N/A	N/A
16	16 Cell	0.633	233	3.79	225
21	16 Cell	0.639	390	3.50	255
22	16 Cell	0.628	238	113.85	129

5.2.3 Specific Impulse Estimation

To gain a measure of performance, the amount of oxidizer was needed to be found to calculate the I_{sp} . The hybrid test fire video footage for all fuel configurations was examined to find the average amount of oxidizer used for each fuel. From cold flow testing, it was found when the casing was loaded with a 9 inch grain with a volume of 21.7 in³ (356 mL) to be 2.98 lbm (1.35 kg). Audio and visual cues from the GoPro camera were used to detect ignition time, burnout time, N₂O flow after firing time, and N₂O flow end time. The burn time of the motor and the N₂O flow after burn time were found using these instances. Figure 5.9 shows a four cell test fire while Appendix G shows the eight and sixteen cells. Table 5.3 shows the results from the video footage.

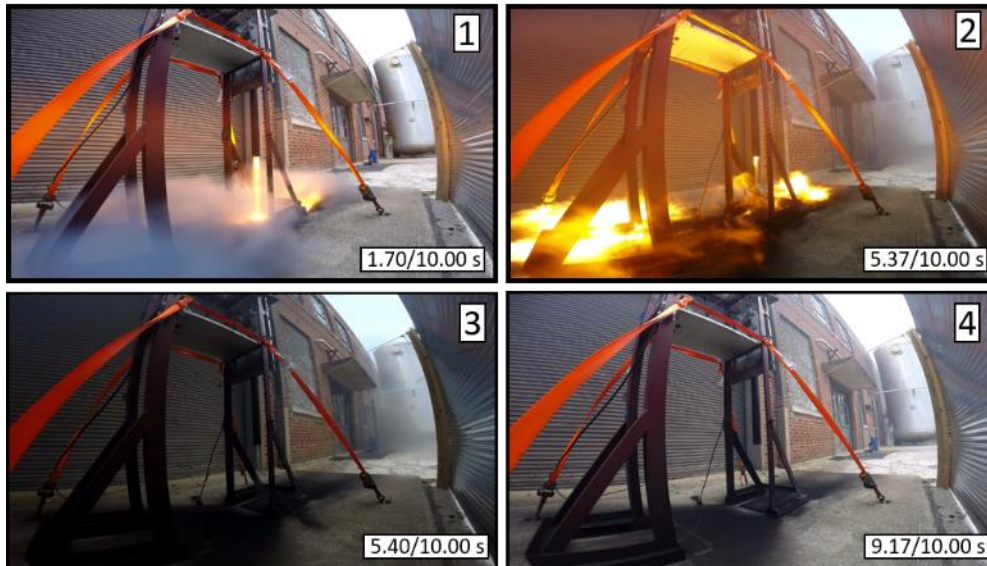


Figure 5.9 Images from Video Footage of the Four Cell Test Fire

Table 5.3 Burn Time and Post Burn Nitrous Flow Time Comparison

Fuel Geometry	Burn Time (s)	Post Burn Nitrous Flow Time (s)
K321 Short	4.23	0.00
Four	3.67	3.77
Eight	3.62	3.92
Sixteen	5.26	1.77

The burn time and post burn N₂O time of all ABS/paraffin configurations show that not all of the oxidizer was used during the test fire while the commercially available motor did use all of the available oxidizer. To estimate the I_{sp} for all four configurations, it was assumed that the mass flow rate of the nitrous during burn and after burn was constant. For instance, the four cell was found to have a burn time and a post burn N₂O flow time of 3.67s and 3.77s respectively. These times were then used with the amount of the oxidizer in the tank, 2.98 lbm, to find the burn oxidizer mass. Finally, equation 5.2 was used to find the I_{sp} using the mass of fuel, m_{fuel} , mass of oxidizer, $m_{oxidizer}$, and gravitational constant, g , were used, and the results were recorded into Table 5.4.

$$I_{sp} = \frac{Impulse}{(m_{fuel} + m_{oxidizer}) \cdot g} \quad (5.2)$$

Table 5.4 Performance Calculations

Test Number	Motor Designation	Fuel Mass (lbm)	Oxidizer Mass (lbm)	O/F Ratio	Specific Impulse (s)
8	K321 Short	0.503	2.98	5.93	86.8
9	K321 Short	0.485	2.98	6.14	86.8
12	4 Cell	0.639	1.47	2.30	185
13	4 Cell	0.626	1.47	2.35	110
14	4 Cell	0.631	1.47	2.33	153
15	8 Cell	0.637	1.43	2.25	144
23	8 Cell	0.639	N/A	N/A	N/A
24	8 Cell	0.646	N/A	N/A	N/A
16	16 Cell	0.633	2.23	3.52	78.8
21	16 Cell	0.639	2.23	3.49	89.2
22	16 Cell	0.628	2.23	3.55	45.3

Table 5.4 shows the four cell and eight cell geometries had a higher performance than the sixteen cells and the PBAN control. However, for the ABS/Paraffin fuel all of these values are far less than what CEA predicted in Figure 4.17. This can easily be seen in Figure 5.10.

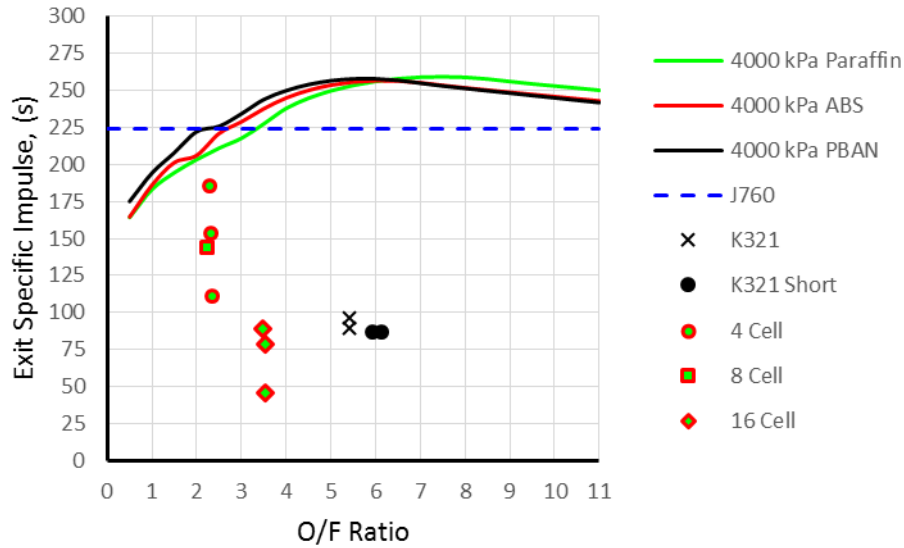


Figure 5.10 CEA Impulse and Tested Impulse Comparison

Notes: The J760 O/F ratio was provided from manufacturer data. The line illustrated for J760 shows the I_{sp} at all O/F ratios due to the lack of information. [45]

The ABS and paraffin test fires were found to be in the O/F range of approximately 2.3 – 3.5 range while the PBAN test fires had an O/F of approximately 6. The CEA calculations do not show these results when using the current nozzle conditions and an assuming chamber pressure from 3200kpa - 4800k Pa. Also, the ABS/paraffin fuel grain's lack of performance was due to the sloughing of the paraffin fuel during the test fire which was clearly visible after some test fires. After some of the eight and sixteen fires, melted paraffin would drip from the nozzle and pool under the test stand which showed some paraffin did not burn in the combustion chamber.

CHAPTER VI

LESSONS LEARNED

6.1 Hardware Modifications

After completing the hybrid test fires, several modifications were considered to improve the future testing of hybrid motors on the existing test stand. The hardware modifications would include a more robust and reliable motor casing, a new ignition device, and a pressurized N₂O system. Finally, these modifications could be used on a horizontal test stand which would allow and a simpler method of motor casing alignment, but would require more raw material to change the current stand's configuration.

6.1.1 Hybrid Motor Casing

The current motor casings were adequate for a couple of test fires, but since they were designed for in-flight use for hobby rockets and not for experimental fuel development, the casings reached the end of their useful life faster than expected. Other drawbacks included, but were not limited to: inability to attach pressure sensors and thermo-couples, the unreliable motor hardware integration using the snap ring design, and uncertainty of ignition of the oxidizer. These drawbacks lead to the design of a custom hybrid casing that would solve all of these problems. Figure 6.1 illustrates the concept for the design.

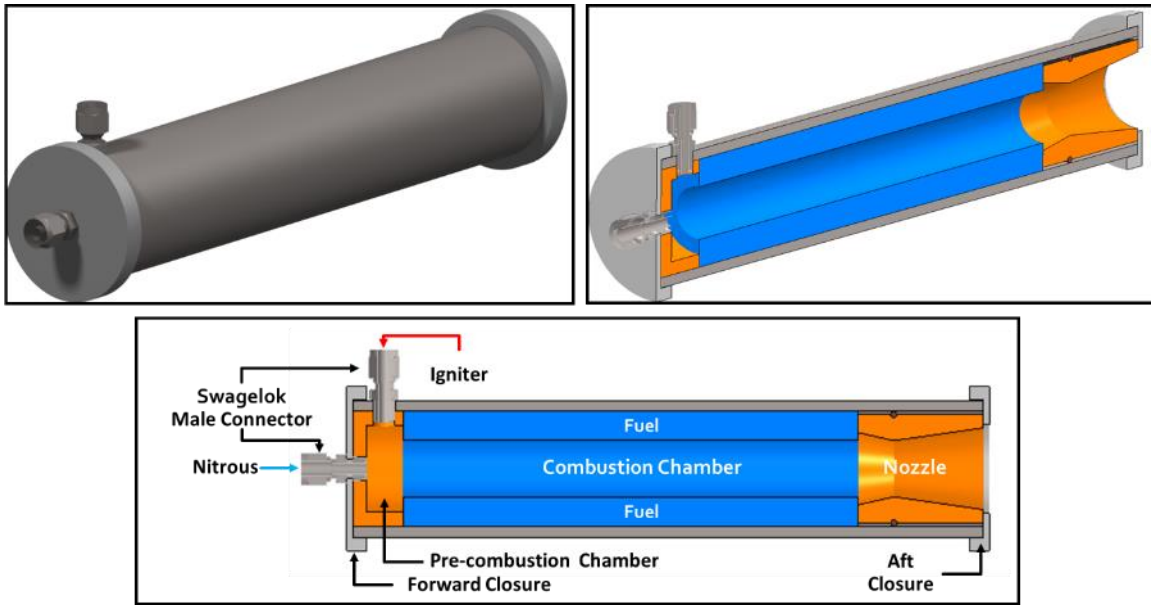


Figure 6.1 New Hybrid Casing Concept

To ensure the new casing would have a longer life cycle than the current casing's design, it should have a $\frac{1}{4}$ in wall thickness and use 4340 alloy steel. The new design uses hardware similar to commercially available Cesaroni solid motor casings, such as threaded forward and aft closures and slightly larger casing inner diameter. Both closures will compress all motor hardware inside the hybrid casing with no gaps. Forward closure will contain a Swagelok male connector, $\frac{1}{4}$ inch tube outer diameter x $\frac{1}{8}$ inch male NPT, to allow N_2O to be injected into the pre-combustion chamber. The pre-combustion chamber will give the system the ability of a more reliable ignition system using another Swagelok male connector. The ignition system, illustrated in Figure 6.2, uses nichrome wire dipped in pyrogen that will be potted with epoxy resin and sealed inside the Swagelok connector. The external lead wires will pass through a crimped section of tubing, and attach to a power source [44]. Pressure taps, and thermocouples would also be added to the system in the

pre-combustion chamber. The new casing requires further research and design, but will offer a more robust and reliable design than the current casing.

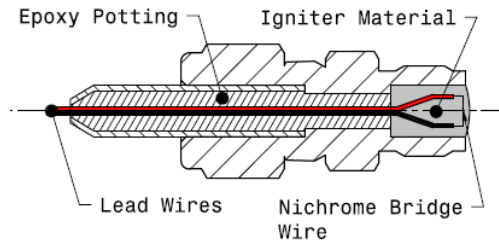


Figure 6.2 Igniter System

Note: This design was used by NASA Ames Research Center. [44]

6.1.2 Nitrogen Oxide Feed System

The new casing design incorporates a top-fed nitrous system as opposed to the current bottom-fed N_2O system. The new N_2O configuration allows the design to be directly fed from an external nitrous system, and would eliminate the presence of an on board N_2O reservoir. The new feed system would require an inert pressurant gas, most likely helium, to ensure an accurate mass flow rate measurements, and pneumatically actuated ball valves to control the oxidizer flow. Further research and design are required to accomplish this task, but could be easily integrated with the current system.

6.1.3 Horizontal Test Stand

Though the MSHVITS system works and could be easily integrated with the new design changes, loading and aligning the motor is difficult and could be simplified if a new horizontal test stand was used. The proposed horizontal test stand would allow an easier integration process using C-clamps and slotted aluminum railing to fix the motor in designated positions. A commercial system from Aerocon Inc uses this design [47],

illustrated in Figure 6.3, and could easily be purchased and modified. Aerocon Systems' test stand is rated for thrust values of 1500 lbf and is designed for 38 – 98 mm diameter motors to be used. The test stand would have to be mounted to the current ground support system or a fixed to a platform.

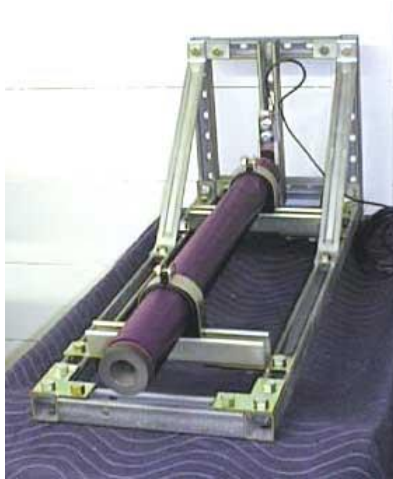


Figure 6.3 Aerocon Systems' Horizontal/Vertical Test Stand

Note: Image from reference [47].

6.2 Fuel Modifications

The current experiments show that the proposed fuel geometries do not use all of the available paraffin which, in turn, hinders the performance. Also, the radial azimuthal geometry's thin outer wall could contribute to unintended burning of the casing which can lead to a rupture. With a new casing design, a thicker outer wall geometry or a phenolic liner could prevent the rupture. To improve performance of the current geometry, the ABS structure would have to become more complex to prevent the sloughing of the paraffin. Previously, the acquired 3D printers couldn't print these complex structures with the single extruder, but with the addition of the dual extruder it is now possible.

6.2.1 Azimuthally and Axially Partitioned Cells

Keeping the same azimuthally design for the four, eight, and sixteen cell geometries but incorporating axial partitions could help contain the paraffin from sloughing and dripping during the burn of the motor. To prevent the loss of the paraffin, the ABS fuel would be partitioned, as shown in Figure 6.4. The ABS partitions would create segments of paraffin fuel which would be similar to the hobby solid propellant fuel grains, but would be held in a single ABS structure. The ABS structure could vary the number of segments and the length of each segment. A small hole will be centered in each partition to allow paraffin to flow in between each segments to initially be filled, but would later be sealed by acetone welding plugs to the exterior fill holes of the motor. Since the TAZ6 now has the capability of a dual extruder, this model could be made using dissolvable build material.

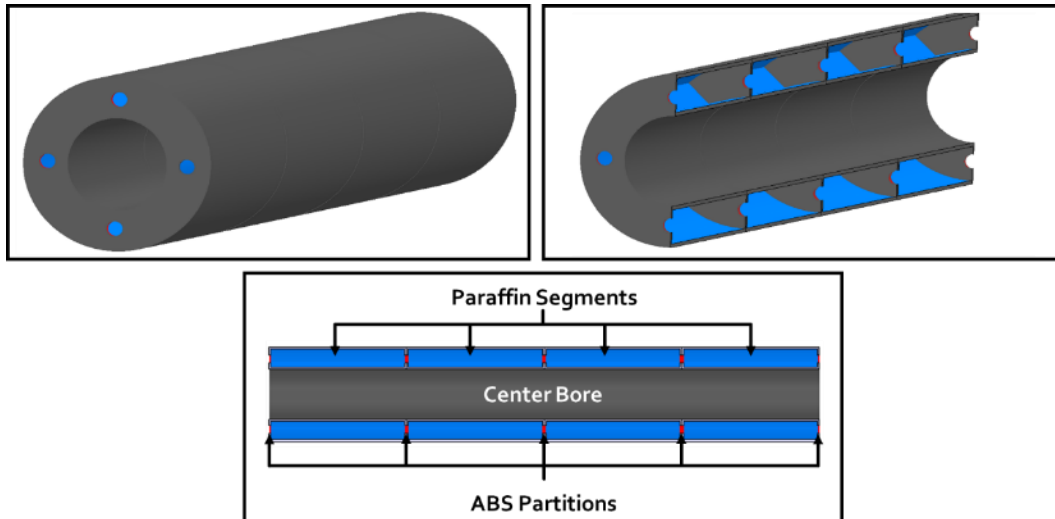


Figure 6.4 Isometric and Cross-sectional View of the Azimuthally and Axially Four Cell Partitioned Design

6.2.2 Helical Design

A helical design was originally the first concept of this project, but due to printer capabilities it was postponed. The design incorporates the same azimuthal design as previously discussed, but follows a spiral pattern. The spiral pattern could contain one or more or less rotations pending on the user's input. Each rotation would affect how the propellant burns, but could improve the structural integrity of the overall grain and may prevent the sloughing of the paraffin. Figure 6.5 shows a four cell geometry with the helical design.

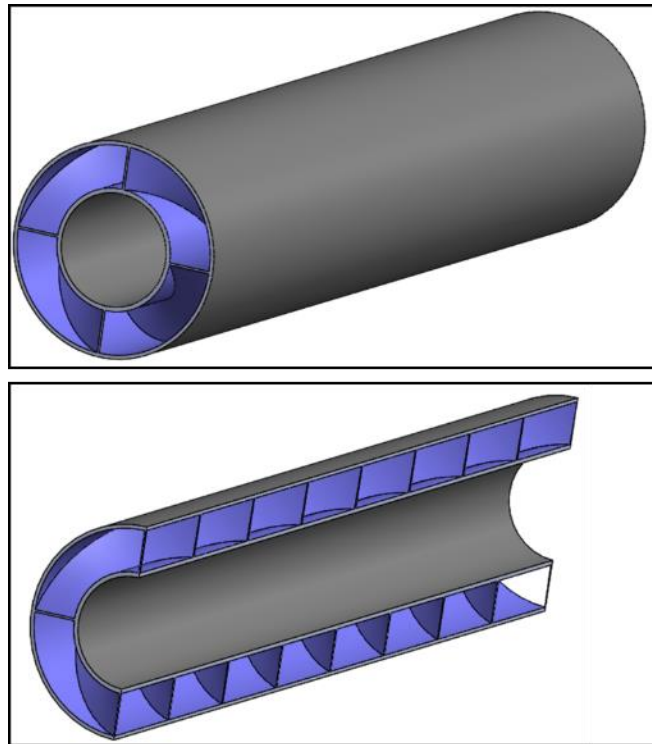


Figure 6.5 Four Cell Helical Design

6.3 Conclusion

It can be concluded that the ABS/paraffin fuel can be used as a successful hybrid fuel. The test fires show the promise of these fuel designs for improved thrust and specific impulse when compared to classic hybrid fuels. To increase the performance, a more complex ABS geometry is required to mitigate the sloughing of the paraffin fuel during the burn. More additives could also be added to the paraffin such as aluminum to increase the performance. It was also found that a more robust and refined test system with more control and measurement capability is needed.

REFERENCES

- [1] M. V. F. Ribeiro and P. C. G. Junior, "Hybrid Rocket Motors Propellants: A Historical Approach," in *21st International Congress of Mechanical Engineering*, Natal, 2011.
- [2] Parabolic Arc, "Virgin Galactic Spins Its Way Back to Rubber Engine for SpaceShipTwo," 20 October 2015. [Online]. Available: <http://www.parabolicarc.com/2015/10/20/virgin-galactic-spins-rubber-engine-spaceshiptwo/>. [Accessed 7 October 2016].
- [3] S. A. Whitmore, Z. W. Peterson and S. D. Eilers, "Analytical and Experimental Comparisons of HTPB and ABS as Hybrid Rocket Fuels," in *47th Joint Propulsion Conference*, San Diego, 2011.
- [4] Space Propulsion Group Inc., "Propellants," 2012. [Online]. Available: <http://www.spg-corp.com/advanced-hybrid-rocket-fuels.html>. [Accessed 7 October 2016].
- [5] AMazing, "What is Additive Manufacturing?," [Online]. Available: <http://additivemanufacturing.com/basics/>. [Accessed 20 8 2016].
- [6] Village Plastics Co, "3D Printing Filament," [Online]. Available: <http://villageplastics.com/products/3d-printing-filament/>. [Accessed 8 18 2016].
- [7] Pub Chem, "1,3 Butadiene," [Online]. Available: https://pubchem.ncbi.nlm.nih.gov/compound/1_3-butadiene#section=Top. [Accessed 18 8 2016].
- [8] Pub Chem, "ACRYLONITRILE," [Online]. Available: <https://pubchem.ncbi.nlm.nih.gov/compound/7855#section=Top>. [Accessed 8 18 2016].
- [9] L.-f. tong, H.-y. Ma and Z.-p. Fang, "THERMAL DECOMPOSITION AND FLAMMABILITY OF ACRYLONITRILE-BUTADIENE-STYRENE/MULTI-WALLED CARBON NANOTUBES COMPOSITES," *Chinese Journal of Polymer Science*, vol. 26, no. 3, pp. 331 - 339, 2008.

- [10] Lulzbot, "LulzBot TAZ 6," 2016. [Online]. Available:
<https://www.lulzbot.com/store/printers/lulzbot-taz-6>.
- [11] Ultimaker, "Cura Software," 2016. [Online]. Available:
<https://ultimaker.com/en/products/cura-software>. [Accessed 23 10 2016].
- [12] L. Galfetti, L. Merotto, M. Boiocchi, F. Maggi and L. T. DeLuca,
"EXPERIMENTAL INVESTIGATION OF PARAFFIN-BASED FUELS
FOR HYBRID ROCKET PROPULSION," in *Progress in Propulsion
Physics*, St. Petersburg, 2013.
- [13] McMaster Carr, "Paraffin Safety Data Sheet," [Online]. Available:
<http://www.mcmaster.com/#1627700-sds-paraffin-081815/=13sm6iz>.
[Accessed 8 19 2016].
- [14] S. E. Dillon and A. Hamins, "IGNITION PROPENSITY AND HEAT FLUX
PROFILES OF CANDLE FLAMES FOR FIRE INVESTIGATION," in
Interscience Communications, London, 2003.
- [15] Contrail Rockets, "54mm Hybrid Rocket Motor Reload Manual," 14 2 2006.
[Online]. Available:
[http://www.contrailrockets.com/Documents/54mm%20Instruction%20Man
ual.pdf](http://www.contrailrockets.com/Documents/54mm%20Instruction%20Manual.pdf). [Accessed 15 1 2016].
- [16] W. R. Patterson, "DEVELOPMENT OF A ROCKET MOTOR TEST SYSTEM
AND A STUDY OF HYBRID ROCKET FUEL GRAINS," Mississippi
State University, Mississippi State, MS, 2009.
- [17] PCB Piezotronics, "Model: 208C04," 2016. [Online]. Available:
<http://www.pcb.com/products.aspx?m=208C04>. [Accessed 15 6 2016].
- [18] National Instruments, "NI USB-6251 Screw Terminal," 2016. [Online]. Available:
<http://sine.ni.com/nips/cds/view/p/lang/en/nid/202802>. [Accessed 8
Septemeber 2016].
- [19] National Instruments, "NI CB-68LP," 2016. [Online]. Available:
<http://sine.ni.com/nips/cds/view/p/lang/en/nid/1187>. [Accessed 8
Sepetember 2016].
- [20] National Instruments, "Model: 484B06," 2016. [Online]. Available:
<http://www.pcb.com/products.aspx?m=484B06>. [Accessed 8 September
2016].
- [21] B. J. McBride and S. Gordon, "Computer Program for Calculations of Complex
Chemical Equilibrium Compositions and Applications II. Useres Manual
and Program Description," NASA, Cleveland, 1996.

- [22] A. V. Mehdi Mehrpooya and F. Gharagheizi, "Prediction of Standard Enthalpy of Formation by a QSPR Model," *International Journal of Molecular Sciences*, vol. 8, pp. 407-432, 2007.
- [23] "NIST," 4 August 2016. [Online]. Available: <http://www.nist.gov/>. [Accessed 1 July 2016].
- [24] J. Brandrup, E. A. Grulke and E. H. Immergut, *Polymer Handbook*, New York: Wiley, 2003.
- [25] D. Van Krevelen, "Chapter 21 Thermochemical Properties," in *Properties of Polymers Correlations With Chemical Structure*, Amsterdam, Elsevier Publishing Company, 1972, pp. 327 - 347.
- [26] D. W. Van Krevelen, "Chapter 20: Thermochemical Properties," in *Properties of polymers : their correlation with chemical structure : their numerical estimation and prediction from additive group contributions*, Fourth ed., Amsterdam, Elsevier, 2009, pp. 749-762.
- [27] National Institute of Standards and Technology, "webbook.nist.gov," 2016. [Online]. Available: <http://webbook.nist.gov/cgi/cbook.cgi?ID=C10024972&Mask=1#Thermo-Gas>. [Accessed July 2016].
- [28] R. Naka, "nakka-rocketry," 28 February 2015. [Online]. Available: <http://www.nakka-rocketry.net/sorb.html#Introduction>. [Accessed July 2016].
- [29] Chemicalland21, "chemicalland21," [Online]. Available: <http://www.chemicalland21.com/lifescience/foco/D-SORBITOL.htm>. [Accessed July 2016].
- [30] National Institute of Standards and Technology, "Webbok.nist.gov," 2016. [Online]. Available: <http://webbook.nist.gov/cgi/cbook.cgi?ID=C50704&Mask=2>. [Accessed July 2016].
- [31] D. W. Van Krevlen, "Thermochemical Properties: Calculation of the Free ENthalpy of Reaction From Group Contributions," in *Properties of Polymers*, Amsterdam, Elsevier, 1990, pp. 629-639.
- [32] M. A. Daniel, "Polyurethane Binder Systems for Polymer Bonded Explosives," Weapons Systems Division, Edinburgh South Australia, 2006.
- [33] R. A. Braunig, "Rocket Propellants," 2008. [Online]. Available: <http://www.braeunig.us/space/propel.htm>. [Accessed July 2016].

- [34] ProPep 3, *PropPep Program*.
- [35] E. J. Prosen and F. D. Rossini, "HEATS OF COMBUSTION AND FORMATION OF THE PARAFFIN HYDROCARBONS AT 25 C," *Research of the National Bureau of Standards*, vol. 34, pp. 263 - 269, 1945.
- [36] J. M. McCulley and S. A. Whitmore, *DESIGN AND TESTING OF DIGITALLY MANUFACTURED PARAFFIN ACRYLONITRILE-BUTADIENE-STYRENE HYBRID ROCKET MOTORS*, Logan: Utah State University, 2012.
- [37] C. E. Carraher, "5.9 Polymers From, 1,4-Dienes," in *Polymer Chemistry*, Boca Raton, CRC Press, 2008, pp. 162-164.
- [38] J. V. Rutowski and B. C. Levin, "Acrylonitrile-Butadiene-Styrene Copolymers (ABS):Pyrolysis and Combustion Products and their Toxicity-A Review of the Literature," *Fire and Materials*, vol. Volume 10, pp. 93 - 105, 1986.
- [39] CHI MEI Corporation, "Certificate of Formula for POLYLAC® PA-747," Department of Product Strategy and Service, Tainan City, 2015.
- [40] NIST, "2-Propenenitrile," [Online]. Available: <http://webbook.nist.gov/cgi/cbook.cgi?ID=C107131&Units=SI&Mask=1#Thermo-Gas>. [Accessed 1 July 2016].
- [41] J. Brandrup, E. H. Immergut and E. A. Grulke, "Table 1.1 With Acyclic Carbons Only In The Main Chain," in *Polymer Handbook*, Fourth Edition ed., New York, John Wiley and Sons, 1998, pp. II 365 - II 373.
- [42] NIST, "1,3- Butadiene," 2016. [Online]. Available: <http://webbook.nist.gov/cgi/cbook.cgi?ID=C106990&Units=SI&Mask=1#Thermo-Gas>. [Accessed 1 July 2016].
- [43] NIST, "Styrene," 2016. [Online]. Available: <http://webbook.nist.gov/cgi/cbook.cgi?ID=C100425&Units=SI&Mask=1#Thermo-Gas>. [Accessed 1 July 2016].
- [44] K. Lohner, J. Dyer, E. Doran and Z. Dunn, "Fuel Regression Rate Characterization Using a Laboratory Scale Nitrous Oxide Hybrid Propulsion System," in *42nd Joint Propulsion Conference*, Sacramento, 2006.
- [45] Cesaroni , "Pro 54 1266J760-19A," [Online]. Available: <http://www.pro38.com/products/pro54/motor/MotorData.php?prodid=1266J760-19A>. [Accessed 20 September 2015].

- [46] Tripoli Rocketry Association INC, "Tripoli," 22 January 2007. [Online]. Available: <http://www.contrailrockets.com/TMTPapers/K321.pdf>. [Accessed 20 April 2016].
- [47] Aerocon Systems, "Horizontal/Vertical Test Stand to 1500 LB-f Thrust," [Online]. Available: <http://aeroconsystems.com/cart/motor-test-stands/horizontal/vertical-test-stand-to-1500-lb-f-thrust/>. [Accessed 6 8 2016].

APPENDIX A
RADIAL FUEL GRAIN CALCULATIONS

Radial Fuel Grain Calculations:

Estimated cross sectional area of inner and outer walls

$$\begin{aligned}
 t_{\text{ring.in}} &:= 1\text{-mm} & t_{\text{ring.out}} &:= 1\text{-mm} & r_{\text{outer}} &:= 24.257\text{-mm} & r_{\text{inner}} &:= 12.7\text{-mm} \\
 A_{\text{outer1}} &:= \pi \cdot r_{\text{outer}}^2 & A_{\text{inner1}} &:= \pi \cdot r_{\text{inner}}^2 & r_{\text{outer2}} &:= r_{\text{outer}} - t_{\text{ring.out}} \\
 r_{\text{inner2}} &:= r_{\text{inner}} + t_{\text{ring.in}} & A_{\text{outer2}} &:= \pi \cdot r_{\text{outer2}}^2 & A_{\text{inner2}} &:= \pi \cdot r_{\text{inner2}}^2 \\
 A_{\text{outer.}} &:= A_{\text{outer1}} - A_{\text{outer2}} = 149.27\text{-mm}^2 & A_{\text{inner.}} &:= A_{\text{inner2}} - A_{\text{inner1}} = 82.938\text{-mm}^2 \\
 A_{\text{ABS.ring}} &:= A_{\text{outer.}} + A_{\text{inner.}} = 232.208\text{-mm}^2 & A_{\text{grain}} &:= A_{\text{outer1}} - A_{\text{inner1}} = 1.342 \times 10^3\text{-mm}^2
 \end{aligned}$$

Estimated cross sectional area for variable cell wall thickness

$$\begin{aligned}
 t_{\text{wall}} &:= 1\text{-mm} & L_{\text{wall}} &:= 9.5605\text{-mm} & A_{\text{wall}} &:= t_{\text{wall}} \cdot L_{\text{wall}} = 9.56\text{-mm}^2 \\
 n_{\text{wall}} &:= 4 & A_{\text{ABS}} &:= A_{\text{ABS.ring}} + A_{\text{wall}} \cdot n_{\text{wall}} = 270.45\text{-mm}^2 & A_{\text{cells}} &:= A_{\text{grain}} - A_{\text{ABS}}
 \end{aligned}$$

$$\text{Infill}\%_{\text{vol}} := \frac{A_{\text{ABS}}}{A_{\text{cells}} + A_{\text{ABS}}} = 20.15556\%$$

$$\text{Vol}_{\text{ABS}} := A_{\text{ABS}} \cdot h_{\text{sample}} = 37.782\text{-mL}$$

Figure A.1 Radial Fuel Grain Calculations

APPENDIX B
SOILD/HYBRID TEST PROCEDURES

Solid/Hybrid Test Procedures

Mississippi State Propulsion Team
Mississippi State University, Mississippi State, MS, 39762

The below procedures are for the 2016 MSHVITS system only. The hybrid or solid motor should be assembled and checked before these procedures are started. The initial part of each section can be performed at the same time, but require multiple ground support personal. Follow all procedures to ensure a safe and reliable test.

Multipurpose Solid/Hybrid Vertically Integrated Test Stand:

- Place test stand on test platform
 - The stand should be placed in the center of the platform
- Secure stand to platform via ratchet straps
 - Each strap should be tight as possible to ensure unwanted movement
 - Place thermal protection over straps
- Integrate rocket to stand
- Tighten top clamp
 - If the clamp is too wide/narrow, loosen the allen bolts, and rotate the cylindrical knob on the back until positioning is correct, and re-tighten allen bolts.
- Tighten center ratchet strap
- Align top of rocket cap with force sensor.
- Tighten bottom U-bolt (if required)
- Align the force sensor front to back with the cap
 - To move this, first, loosen the alignment allen bolts on the force sensor assembly.
- Pre-tension should be done after nitrous testing and performed slowly applying tension (see data section for further instructions)

Nitrous System:

- Only applicable for **hybrid** testing. If testing solid skip to the next section.
- Fill the bottles by first freezing the smaller bottle. Connect both hose ends, and open the mother bottle first. Then open daughter bottle. Wait until gas transfer is no longer heard. Close the daughter and then mother bottle, and slowly detach the hose, allowing pressure to release.
 - If mass does not transfer, the mother bottle may be empty, or the daughter bottle full.
- Setup the solenoids in-between the test stand and the steel pole next to the door.
- Roll out the power cables from the door to the test stand. Cable ends with clips should be away from the solenoids.
- Attach the wire to the solenoids by screwing the wire nuts onto the wires. The black and white wire connect to the flow solenoid (has a blue screw-on output) while the pink and green connect to the purge solenoid (has a silver barb output).

- Place the control box on top of the battery. Connect the wires inside the box horizontally with the bolts. The left-most wire is a common ground, and connects to the right, black ground side of the battery. The shorter, middle wire connects to the red, positive on the left.
- Connect the wires to the back of the control box using the wing nuts. Both the smaller yellow and larger blue connector are connected to the common ground, the larger bolt on the left near the edge of the box.
- Connect the positive for the flow solenoid, the second larger blue connector, to the larger bolt near the center of the box. It doesn't matter which of the two blue connectors is attached.
- Connect the positive for the purge solenoid, the second smaller yellow connector, to the smaller bolt in between the two larger bolts. It doesn't matter which yellow end is attached to positive or ground.
- Put the bottle in the bucket and strap down to the pole. Attach the bottle to the solenoids.
- Connect the nitrous fill line to the solenoids. DO NOT YET CONNECT ROCKET FILL LINE TO NITROUS LINE. Secure the end of the nitrous fill line.
- Connect the purge line.
- Open up the bottle, pressurizing the line. Test the fill (Right, silver switch) and purge (middle, covered switch).
- CLOSE THE BOTTLE. PURGE THE LINE, OR DISCONNECT BOTTLE UNTIL JUST BEFORE TESTING.
- Connect the rocket fill line to the nitrous fill line. The bottle should NOT be open yet.
- Have all personal leave the area. Reconnect (if disconnected before) and reopen the bottle.
- Test firing: Flip the fill switch on. Leave on until just after ignition. Once ignition has occurred turn fill line off.
- After test fire has completed: close the bottle and purge the system at which point the nitrous bottle could be disconnected for replacement if necessary.

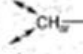
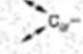
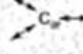
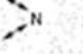



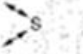
Data Acquisition System:

- Open the labview file. Running it should make data appear on the voltage graph. Ensure that the daq is plugged in and running, and is connected to the output of the signal conditioner. If the force sensor is not yet attached, the graph should be reading out a constant 11v.
 - If the program has an error, it most likely hasn't identified the daq. Make sure the daq is detected by the computer.
 - If spikes occur during testing, ensure that the three connections (signal conditioner output and ground, and resistor) are sound. Reset, re-calibrate, and self-test the daq using NI Max.
 - If the daq has to be swapped out, the sub-vi used to pull information from the daq will have to be rebuilt. Open the back panel, and click on the daq assistant. Look under voltage channels, and right-click the voltage measurement. Select "change physical channel" and select channel a0 on the new daq.

- Attach the force sensor. Ensure that the force sensor is properly screwed into the sensor plate, and that the white force sensor cable is properly positioned, protected from thrust and thrust stand hardware, and attached.
 - The pad on top of the force sensor and the screw on the bottom of the force sensor can both become loose. This is okay, just hand-tighten the pad, and use a screwdriver to tighten the screw.
- Check to see that the force sensor responds appropriately on the graph. Press the sensor and the stand to check for force increases.
- Clear the graph by pressing the stop-sign ICON (not stop button). Restart the program and watch for an average value on the right side set of values. Choose this as a starting point for adding pre-tension.
 - The starting value at 1. If values are below the x-axis before tensioning, merely twist the knob on the front of the conditioner until it is a tenth of a volt or two above 0. Use this value as the pretension starting point. Do not use the knob during pretension.
- Add $50 \text{ lb} \cdot 0.005$ to this value, since each pound is equal to 5 millivolts. The target value is 1.25. Add tension until the graph or value array reaches approximately this target value. More pretension can be added to the system if required, but all testing should stay consistent.
- Restart the program to clear the graph before testing.

APPENDIX C
VAN KREVLAN GROUP CONTRIBUTIONS

TABLE 20.1 Free enthalpy of formation of some small molecules and related group contributions to the free enthalpy of formation of large molecules

Group	$\Delta G_f^\circ(T)$ (J/mol)	Group	$\Delta G_f^\circ(T)$ (J/mol)
CH ₄	-79,000 + 92.5 T	H ₂ O	-243,000 + 48.2 T
-CH ₃	-46,000 + 95 T	-OH	-176,000 + 50 T
-CH ₂ -	-22,000 + 102 T	-O-	-120,000 + 70 T
>CH-	-2,700 + 120 T	H ₂ C=O	-118,000 + 26 T
>C<	20,000 + 140 T	-HC=O	-125,000 + 26 T
=CH ₂	23,000 + 30 T	>C=O	-132,000 + 40 T
=CH-	38,000 + 38 T	HCOOH	-381,000 + 100 T
-C<	50,000 + 50 T	-COOH	-393,000 + 118 T
=C-	147,000 - 20 T	-COO-	-337,000 + 116 T
≡CH	112,500 - 32.5 T	NH ₃	-48,000 + 107 T
≡C<	115,000 - 25 T	-NH ₂	11,500 + 102.5 T
	12,500 + 26 T	-NH-	58,000 + 120 T
	25,000 + 38 T	>N-	97,000 + 150 T
	21,000 + 21.5 T		69,000 + 50 T
	75,000 + 156 T	H ₂ S	-25,000 - 30 T
	87,000 + 167 T	-SH	13,000 - 33 T
	100,000 + 180 T	-S-	40,000 - 24 T
HF	-270,000 - 6 T		60,000 - 60 T
-F	-195,000 - 6 T	-S-S-	46,000 - 28 T
		>S=O	-63,000 + 63 T
		-SO ₂ -	-282,000 + 152 T
		-NO ₂	-41,500 + 143 T
		-ONO	-21,000 + 130 T
		-ONO ₂	-88,000 + 213 T
		3-ring	100,000 - 122 T

(continued)

Table 20.1 (continued)

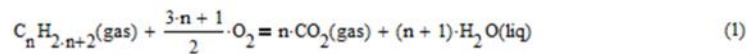
Group	$\Delta G_f^\circ(T)$ (J/mol)	Group	$\Delta G_f^\circ(T)$ (J/mol)
HCl	-93,000 - 9 T	4-ring	100,000 - 110 T
-Cl	-49,000 - 9 T	5-ring	20,000 - 100 T
HBr	50,000 - 14 T	6-ring	-3,000 - 70 T
-Br	-14,000 - 14 T	Conjugation of double bonds	-18,000 + 16 T
HI	12,000 - 41 T	<i>cis-trans</i> Conversion	-6,000 + 7 T
-I	40,000 - 41 T		
HCN	130,000 - 34.5 T		
-CN	123,000 - 28.5 T		
C ₂ O ₂	-92,000 - 59 T	N ₂ O	81,000 + 75 T
CO	-111,000 - 90 T	NO	90,500 - 13 T
CO ₂	-394,500 - 2 T	NO ₂	33,000 + 63 T
COCl ₂	-221,000 + 47 T	HNO ₂	-130,000 + 208 T
COS	-140,000 - 85 T	NOCl	53,000 + 48 T
CS ₂	-111,500 - 152 T	N ₂ H ₄	92,000 + 223 T
S ₂ (g)	130,000 - 164 T	Br ₂ (g)	31,000 - 93 T
SO ₂	-300,000 + 0 T	I ₂ (g)	63,000 - 144 T
SO ₃	-400,000 + 95 T	(CN) ₂	310,000 - 44 T
SOCl ₂	-215,000 + 59 T	H ₂ O ₂	-138,000 + 108 T
SO ₂ Cl ₂	-360,000 + 158 T	O ₃	142,000 + 70 T

APPENDIX D
PARAFFIN HEAT OF FORMATION CALCULATIONS

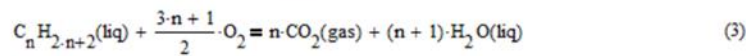
HEATS OF COMBUSTION AND FORMATION OF THE
PARAFFIN HYDROCARBONS AT 25 C

By Edward J. Prosen and Frederick D. Rossini

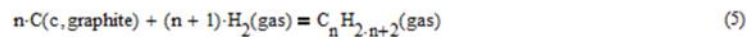
cal = 4.187-J kJ := 1000-J MJ := 10⁶-J Square roots are +/- uncertainties. Eq's valid for n > 5.



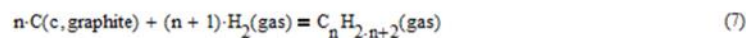
$$\Delta H_{c_g}(n) := (57.909 + 157.443 \cdot n) \cdot \frac{kcal}{mol} \quad \sqrt{0.1647 - 0.03902 \cdot n + 0.002684 \cdot n^2} \quad (2)$$



$$\Delta H_{c_l}(n) := (57.430 + 156.263 \cdot n) \cdot \frac{kcal}{mol} \quad \sqrt{0.1653 - 0.03916 \cdot n + 0.002694 \cdot n^2} \quad (4)$$



$$\Delta H_{f_g}(n) := (-10.408 - 4.926 \cdot n) \cdot \frac{kcal}{mol} \quad \sqrt{0.1648 - 0.03884 \cdot n + 0.002893 \cdot n^2} \quad (6)$$



$$\Delta H_{f_l}(n) := (-10.887 - 6.106 \cdot n) \cdot \frac{kcal}{mol} \quad \sqrt{0.1654 - 0.03898 \cdot n + 0.002903 \cdot n^2} \quad (8)$$

$$i := 0..2 \quad n_i := 15 + 5 \cdot i$$

$$hcl_i := \Delta H_{c_l}(n_i) \quad hcg_i := \Delta H_{c_g}(n_i) \quad hfl_i := \Delta H_{f_l}(n_i) \quad hfg_i := \Delta H_{f_g}(n_i)$$

$$Hc^{(0)} := hcl \quad Hc^{(1)} := hcg \quad Hf^{(0)} := hfl \quad Hf^{(1)} := hfg \quad \text{"0" means not in table.}$$

equatio	Table 2	equatio	Table 2
$Hc = \begin{pmatrix} 2401.38 & 2419.55 \\ 3182.69 & 3206.77 \\ 3964.01 & 3993.98 \end{pmatrix} \cdot \frac{kcal}{mol}$	$\begin{pmatrix} 2401.37 & 2419.55 \\ 3182.69 & 3206.77 \\ 0 & 0 \end{pmatrix} \cdot \frac{kcal}{mol}$	$Hf = \begin{pmatrix} -102.48 & -84.30 \\ -133.01 & -108.93 \\ -163.54 & -133.56 \end{pmatrix} \cdot \frac{kcal}{mol}$	$\begin{pmatrix} -102.49 & -84.31 \\ -133.01 & -108.93 \\ 0 & 0 \end{pmatrix} \cdot \frac{kcal}{mol}$
$Hc = \begin{pmatrix} 10.0541 & 10.1302 \\ 13.3253 & 13.4261 \\ 16.5965 & 16.7220 \end{pmatrix} \cdot \frac{MJ}{mol}$		$Hf = \begin{pmatrix} -429.05 & -352.94 \\ -556.87 & -456.06 \\ -684.70 & -559.18 \end{pmatrix} \cdot \frac{kJ}{mol}$	

APPENDIX E

CHIMEI CORPORATION PA-747 GENERAL ABS

Certificate of Formula for POLYLAC[®] PA-747

We hereby certify that the POLYLAC[®] PA-747 General ABS resin produced by CHIMEI CORPORATION contains the following composition:

Ingredient	Weight Percentage(%)
Acrylonitrile	20~24
Butadiene	19~23
Styrene	54~58
Additive	1~2

Department of Product Strategy & Service



APPENDIX F
THRUST EXTRACTION MATHCAD PROGRAM

```

detmod(data, num, per, time) :=
  sum ← 0
  j ← 0
  z ← 1
  data_time ←  $\frac{\text{time}}{0.001}$ 
  for i ∈ 0..num - 1
    sum ← sum + datai
  avg ←  $\frac{\text{sum}}{\text{num}} \left( \frac{1}{0.005} \right)$ 
  avg_mod ←  $\frac{\text{sum}}{\text{num}}$ 
  data_mod ←  $\frac{\text{data}}{0.005} - \text{avg}$ 
  data_L ← length(data)
  thr ← Stdev(data_mod)·(per)
  j_found ← data_L
  while j ≤ data_L
    | j_thr ← j if data_modj ≥ thr
    | (break) if data_modj ≥ thr
    | j ← j + 1
  while z ≤ data_time - 1
    | data_newz ← data_modj_thr
    | z ← z + 1
    | j_thr ← j_thr + 1
  output ← data_new

```

APPENDIX G
EIGHT AND SIXTEEN CELL TEST FIRE

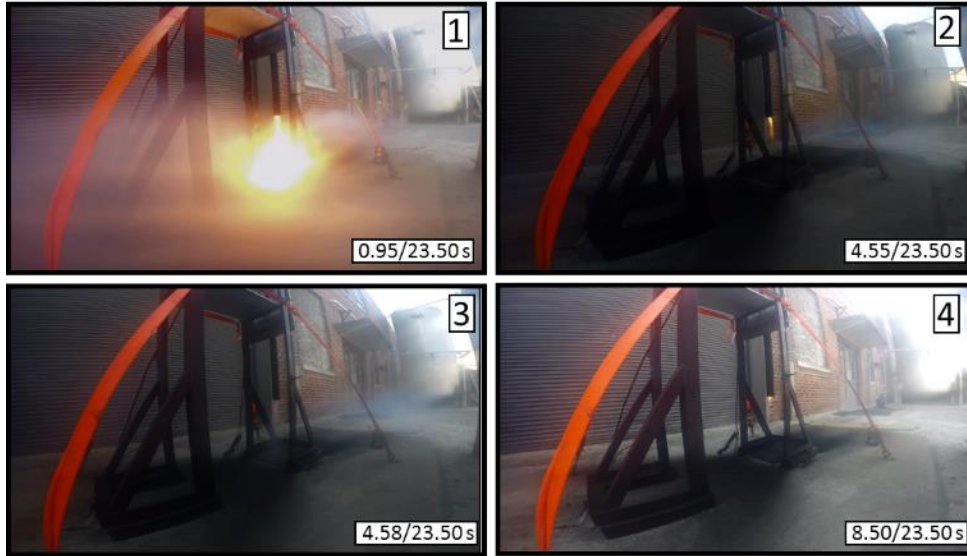


Figure G.1 Eight Cell Test Fire

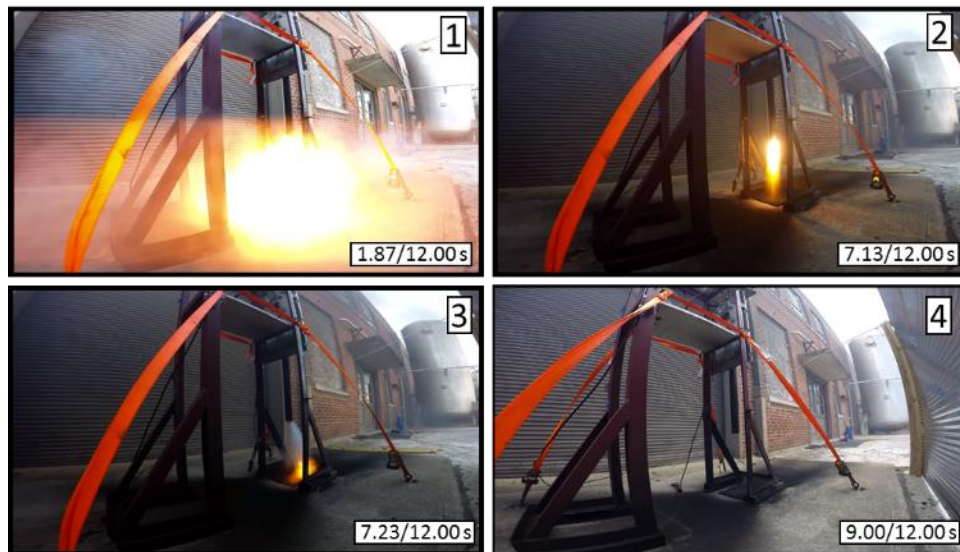


Figure G.2 Sixteen Cell Test Fire